

SAND REPORT

SAND2002-8511
Unlimited Release
November 2002

Thermal Analysis of a H1616 Shipping Container in Hypothetical Accident Conditions

J. T. Hollenshead

Prepared by
Sandia National Laboratories
Albuquerque, New Mexico 87185 and Livermore, California 94550

Sandia is a multiprogram laboratory operated by Sandia Corporation,
a Lockheed Martin Company, for the United States Department of
Energy under Contract DE-AC04-94AL85000.

Approved for public release; further dissemination unlimited.



Sandia National Laboratories

Issued by Sandia National Laboratories, operated for the United States Department of Energy by Sandia Corporation.

NOTICE: This report was prepared as an account of work sponsored by an agency of the United States Government. Neither the United States Government, nor any agency thereof, nor any of their employees, nor any of their contractors, subcontractors, or their employees, make any warranty, express or implied, or assume any legal liability or responsibility for the accuracy, completeness, or usefulness of any information, apparatus, product, or process disclosed, or represent that its use would not infringe privately owned rights. Reference herein to any specific commercial product, process, or service by trade name, trademark, manufacturer, or otherwise, does not necessarily constitute or imply its endorsement, recommendation, or favoring by the United States Government, any agency thereof, or any of their contractors or subcontractors. The views and opinions expressed herein do not necessarily state or reflect those of the United States Government, any agency thereof, or any of their contractors.

Printed in the United States of America. This report has been reproduced directly from the best available copy.

Available to DOE and DOE contractors from
U.S. Department of Energy
Office of Scientific and Technical Information
P.O. Box 62
Oak Ridge, TN 37831

Telephone: (865) 576-8401
Facsimile: (865) 576-5728
E-Mail: reports@adonis.osti.gov
Online ordering: <http://www.doe.gov/bridge>

Available to the public from
U.S. Department of Commerce
National Technical Information Service
5285 Port Royal Rd
Springfield, VA 22161

Telephone: (800) 553-6847
Facsimile: (703) 605-6900
E-Mail: orders@ntis.fedworld.gov
Online ordering: <http://www.ntis.gov/ordering.htm>



SAND2002-8511
Unlimited Release
Printed November 2002

Thermal Analysis of a H1616 Shipping Container in Hypothetical Accident Conditions

Jeromy Todd Hollenshead
Thermal/Fluid Modeling Department
Sandia National Laboratories
Livermore, CA 94551-0969
jtholle@sandia.gov

November 21, 2002

Abstract

The thermal response of the H1616 transport container is simulated to demonstrate compliance with the Federal regulations for performance during hypothetical accident conditions (HAC). The goal is to show that tests conducted for the certification of the H1616 shipping container provide conservatively high estimates of temperatures at key regions within the container. A one-dimensional computational model is developed to simulate the thermal response of the shipping container in cylindrical coordinates. The model assumes the container is axisymmetric and allows for variable thermal properties. The model is calibrated using temperature data obtained from two experimental thermal tests and is then used to evaluate the thermal response of the shipping container to several different scenarios that meet or exceed the Federal regulations. A pre-heating technique, which is used to simulate the thermal effects of a radioactive heat source within the container, is also evaluated.

Intentionally Left Blank

Contents

1	Introduction	7
2	Model Development and Validation	9
3	Model Calibration	13
4	Analysis and Results	21
	Simulation of Thermal Tests including an Internal Heat Source.....	21
	Simulation of Thermal Tests at an Elevated Cooling Temperature	26
	Simulation of Thermal Tests undergoing Solar Insolation	34
5	Conclusions	41
	References	45

Figures

1	Idealized Cross Section of Shipping Container.	8
2	Experimentally Observed Temperature Histories during the C6 Thermal Test.	14
3	Experimentally Observed Temperature History during the C9 Thermal Test.	14
4	Calibration to the C6 Thermal Test using only the Heat Transfer Coefficients.	15
5	Calibration to the C6 Thermal Test including Foam Fire Effects.....	16
6	Shipping Container and Shroud Placement during Thermal Tests.	18
7	Final Calibration Results using the C6 Thermal Test Data.	18
8	Final Calibration Results using the C9 Thermal Test Data.	20
9	Steady-State Temperature Profiles for Different Values of Internal Heat Flux.	23
10	Initial Steady-State Temperature Distribution (C9SIM vs. HSSIM1).	23
11	Temperature Histories for Simulated Thermal Tests (C9SIM vs. HSSIM1)...	24
12	Flange Temperatures for Simulated Thermal Tests (C9SIM vs. HSSIM1)...	24
13	Temperature Differences for Simulated Thermal Tests (C9SIM vs. HSSIM1).	25
14	Initial Steady-State Temperature Distribution (C9SIM vs. HSSIM2).	27
15	Temperature Histories for Simulated Thermal Tests (C9SIM vs. HSSIM2)...	27
16	Flange Temperatures for Simulated Thermal Tests (C9SIM vs. HSSIM2)...	28
17	Temperature Differences for Simulated Thermal Tests (C9SIM vs. HSSIM2).	28
18	Temperature Histories for Simulated Thermal Tests (C9SIM vs. CTSIM1). ..	29
19	Flange Temperatures for Simulated Thermal Tests (C9SIM vs. CTSIM1). ..	29
20	Temperature Differences for Simulated Thermal Tests (C9SIM vs. CTSIM1).	30
21	Temperature Histories for Simulated Thermal Tests (C9SIM vs. CTSIM2). ..	31
22	Flange Temperatures for Simulated Thermal Tests (C9SIM vs. CTSIM2). ..	31
23	Temperature Differences for Simulated Thermal Tests (C9SIM vs. CTSIM2).	32
24	Temperature Histories for Simulated Thermal Tests (C9SIM vs. CTSIM3). ..	33

25	Flange Temperatures for Simulated Thermal Tests (C9SIM vs. CTSIM3). . .	33
26	Temperature Differences for Simulated Thermal Tests (C9SIM vs. CTSIM3).	34
27	Temperature Histories for Simulated Thermal Tests (C9SIM vs. ISSIM1). . .	35
28	Flange Temperatures for Simulated Thermal Tests (C9SIM vs. ISSIM1). . . .	36
29	Temperature Differences for Simulated Thermal Tests (C9SIM vs. ISSIM1)..	36
30	Temperature Histories for Simulated Thermal Tests (C9SIM vs. ISSIM2). . .	37
31	Flange Temperatures for Simulated Thermal Tests (C9SIM vs. ISSIM2). . . .	38
32	Temperature Differences for Simulated Thermal Tests (C9SIM vs. ISSIM2)..	38
33	Temperature Histories for Simulated Thermal Tests (C9SIM vs. ISSIM3). . .	40
34	Flange Temperatures for Simulated Thermal Tests (C9SIM vs. ISSIM3). . . .	40
35	Temperature Differences for Simulated Thermal Tests (C9SIM vs. ISSIM3)..	41

Tables

1	Layer Characteristics of the Shipping Container.	8
2	Selected Properties of Materials within the Shipping Container.	10
3	Thermal Properties of the Polyurethane Foam.	10
4	Thermal Properties of the Packing Material.	11
5	Thermal Properties of the Thermal Barrier.	11
6	Thermal Properties of 304 Stainless Steel.	11
7	Final Model Parameters determined through Calibration.	19
8	System Properties Predicted from Thermal Calibration Tests.	19
9	Description and Results of the C9 Simulation Scenarios.	39

Thermal Analysis of a H1616 Shipping Container in Hypothetical Accident Conditions

1 Introduction

During the spring of 2001, personnel from organization 8243 were finalizing the Safety Analysis Report for Packaging (SARP) for the H1616 shipping container when it was observed that the hypothetical accident condition (HAC) scenario as defined in the Federal requirements document [2] had not been tested for correctly. The requirements call for the container to be placed in a high temperature environment where the temperature exceeds 1475°F, such as in a pool fire or heat radiation facility, for thirty minutes. The requirements then specify that the container should be placed in an ambient temperature of 100°F and exposed to twelve hours of solar insolation followed by twelve hours without insolation. This pattern of solar insolation should be repeated until the temperature reaches steady-state.

In the actual experimental tests conducted for the SARP, containers were placed in a high temperature environment for thirty minutes, but then were removed and allowed to cool at an ambient temperature of approximately 40°F and without solar insolation. Additionally, the experiments were conducted on shipping containers without an internal heat source. In actual conditions, a heat generation source of up to 6.5 Watts would be present within the container. In order to simulate the thermal effects of a heat source, the empty shipping containers were heated to an elevated temperature of 160°F before the thermal tests were conducted.

The goal of this project is to show compliance of the H1616 shipping container with Federal regulations by simulating the container's thermal response under the specified conditions. A one-dimensional finite difference model of the shipping container is developed in cylindrical coordinates. The model assumes the container is axisymmetric and allows for variable thermal properties in the radial direction. The model is first calibrated using the data obtained from thermal experiments and then used to demonstrate that the thermal performance of the shipping container meets or exceeds the requirements. The maximum temperature reached by the O-ring located near the flange of the containment vessel is used as the key measure of the systems thermal response. The following analysis evaluates whether pre-heating shipping containers before the thermal experiments suitably takes into account the lack of the heat generation source on the maximum temperature reached by this O-ring. The analysis also evaluates the difference in the maximum temperature reached at the O-ring between the conditions as tested (cooling at 40°F with no solar insolation) and those specified by the Federal requirements (cooling at 100°F with solar insolation).

This report is divided into sections. Section 2 describes the geometry of the shipping

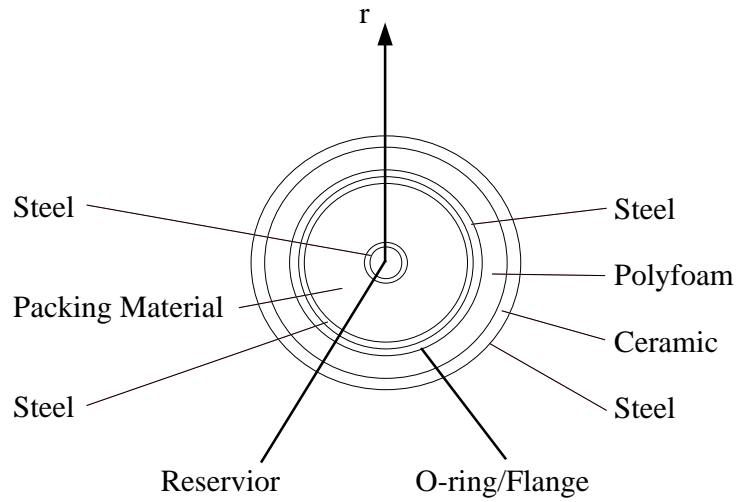


Figure 1. Idealized Cross Section of Shipping Container (Top View).

container and outlines the methodology used to develop and validate the numerical model. Section 3 discusses the calibration of the thermal model using temperature data from two thermal experiments. Section 4 then details the simulation of thermal tests for several different scenarios and discusses the results. The results are then summarized in Section 5.

Table 1. Layer Characteristics of the Shipping Container.

Thickness (inch)	Radius (inch)	Thickness (m)	Radius (m)	Material
1.500	1.500	0.038100	0.038100	Air
0.250	1.750	0.006350	0.044450	Stainless Steel
4.305	6.055	0.109347	0.153797	Packing Material
0.135	6.190	0.003429	0.157226	Stainless Steel
0.030	6.220	0.000762	0.157988	Stainless Steel
0.970	7.190	0.024638	0.182626	Polyurethane Foam
0.500	7.690	0.012700	0.195326	Thermal Barrier
0.048	7.738	0.001219	0.196545	Stainless Steel

2 Model Development and Validation

The H1616 transport container consists of an eighteen gauge insulated stainless steel drum approximately 21.5 inches in length and 16.5 inches in diameter. At the center of the container is a stainless steel vessel known as the reservoir that is spherical and has an approximate diameter of 3.0 inches. When in use, this inner vessel contains a radioactive material that produces decay heat which contributes to the thermal loading of the system. Surrounding the reservoir is a thick layer of packing material made from aluminum tubing. Both the reservoir and packing material are contained within a 304 stainless steel containment vessel. The containment vessel is placed within the outer stainless steel drum and the air space between is filled with a polyurethane foam. A one half inch thick layer of ceramic fiber lines the inside of the outer steel drum to provide an additional thermal barrier.

Although the geometry of the shipping container is known completely, the current analysis describes the flow of heat through the container as a one-dimensional axisymmetric problem in cylindrical coordinates. While this greatly simplifies the problem, it also increases the level of uncertainty associated with the results. Increasing the complexity of the shipping container geometry would help to decrease the level of uncertainty in the results, but would require additional time and funding which are not available. It is therefore assumed the thermal description of the problem is suitable and adequately describes the geometry and physical processes of interest. Figure 1 shows the idealized cross-section of the shipping container in cylindrical coordinates. The various layers that make up the container, their radial thicknesses, and the distance of each layer from the center of the container are shown in Table 1.

The origin of the coordinate system is chosen to be the at the center of the reservoir within the shipping container. The flow of heat is described using the differential energy balance equation[3] :

$$\frac{1}{r} \frac{\partial}{\partial r} \left(kr \frac{\partial T}{\partial r} \right) + q = \rho C_p \frac{\partial T}{\partial t}, \quad (1)$$

where k is the thermal conductivity, q is a volumetric heat generation term, and C_p is the specific heat at constant pressure. The associated initial temperature distribution:

$$T(0, x) = g(x), \quad (2)$$

and boundary conditions on the inside(a):

$$-k \frac{\partial T}{\partial r} |_a = h_a (T_a - T_\infty) - q_a, \quad (3)$$

and outside(b) of the shipping container:

$$-k \frac{\partial T}{\partial r} |_b = h_b (T_b - T_\infty) - q_b + \epsilon \sigma (T_b^4 - T_\infty^4), \quad (4)$$

Table 2. Selected Properties of Materials within the Shipping Container.

Material	Density (kg/m ³)	Solar Absorptivity
Stainless Steel	8083	0.37
Packing Material	401	–
Polyurethane Foam	264	–
Ceramic Thermal Barrier	60	–

Table 3. Thermal Properties of the Polyurethane Foam.

Temperature (C)	C _p (J/g °C)	k (Btu in. / hr ft ² °F)
25	1.35	0.34
50	1.83	–
100	2.46	–
150	3.12	–

are also required to determine the temperature distribution within the container at any time. During the simulation, the values of the parameters in Eqs. (3) and (4) are modified to simulate conditions specified by the Federal requirements. These equations are discretized using a finite volume scheme. The thermal properties of materials within the shipping container vary as a function of temperature and are tabulated in the original SARP report [6] at a number of discrete temperatures. These values are used to linearly interpolate property values at temperatures between the reported values. Properties at temperatures outside the range of the provided values are evaluated at the highest or lowest temperature available. Tables 2 – 4 show the thermal and other relevant properties of interest for the materials used within the shipping container.

A computational program written in FORTRAN is used to solve the equations describing flow using a scheme that is explicit in time and implicit in position. This formulation yields a tri-diagonal matrix that is solved using the Thomas algorithm [5] at each time step. The total number of volume elements in the radial direction is increased to discretize the spatial domain into smaller and smaller elements until the solution converges. The final model is comprised of 1000 volume elements. The uniform time step used in the program is also systematically reduced until no appreciable change in the solution is observed. At each time step, physical properties are evaluated iteratively, starting with the temperature determined at the last time step and continuing until the temperatures used to calculate the physical properties converge to the temperature profile at the new time step. The developed model is validated by comparing the steady-state numerical solution with an analytical solution determined using a thermal resistance model [3]. Once the model is validated, thermal properties within the model are determined from experimental thermal tests. The calibration methodology is described in the following section.

Table 4. Thermal Properties of the Packing Material.

Temperature (C)	C_p (kJ/Kg °K)	k (W / m °F)
27	0.96	0.35

Table 5. Thermal Properties of the Thermal Barrier.

Temperature (F)	C_p (Btu/ lb °F)	k (Btu in. / hr ft ² °F)
400	0.39	0.235
800	0.52	0.261
1200	0.67	0.274
1600	0.84	0.283

Table 6. Thermal Properties of 304 Stainless Steel.

Temperature (K)	C_p (J/kg K)	k (W/m K)	Emissivity (ϵ)
100	272	9.2	–
200	402	12.6	–
300	477	14.9	–
400	515	16.6	–
600	557	19.8	–
800	582	22.6	0.33
1000	611	25.4	0.40
1200	640	28.0	–

Intentionally Left Blank

3 Model Calibration

In order to ensure the thermal performance of the H1616 shipping container satisfied the Federal requirements for hypothetical accident conditions (HAC), several field experiments were conducted for the previous SARP in both radiant heat facilities and in fuel pool fires. In the current analysis, data from two thermal tests conducted in radiant heat facilities is used to calibrate the numerical model. These data are used to estimate the parameters, such as the heat transfer coefficients (h_a, h_b), that appear in Eqs. (3) and (4).

Before the heating portion of the thermal test is initiated, the containers are pre-heated in a 160°F oven until steady-state conditions are reached. This procedure is designed to compensate for the elevated temperatures that would be present in a filled container due to the internal heat source. The containers are then exposed to temperatures over 1475°F for approximately thirty minutes. The ambient temperature is then reduced and the container is allowed to cool and come to thermal equilibrium with its surroundings. Thermocouples placed on the sides of the drum and at various locations of interest within the container itself continuously record temperatures throughout the thermal test. Additionally, blackout indicators, which turn black once they are exposed to a specified maximum temperature, are located in several locations throughout the container during testing. A more complete description of the experimental procedures and a complete record of additional tests that were conducted may be found in the original SARP report [6].

Figure 2 shows temperature data from the C6 test, the first thermal test. Since the actual electronic data files are not available, discrete temperature values from both the shroud and the flange are read from figures contained within the SARP report [6]. The observed flange temperatures are shown in green and the shroud temperatures are shown in red. In the C6 thermal experiment, radiant heat lamps are switched on at around five minutes into the experiment, and the shroud temperature quickly rises above the required temperature of 1475°F to 1525°F. After thirty minutes the heat lamps are turned off and the system is allowed to cool at the ambient temperature, which is assumed to be around 40°F. The maximum flange temperature recorded in the experiment is 344.7°F. During the C9 thermal test, only the shroud temperature history, which is shown in Figure 3, is recorded. The test is conducted in essentially the same fashion as the C6 test with the exception that the shroud reaches a temperature of 1850°F. The maximum recorded flange temperature is 465°F.

The model is first calibrated using the data from the C6 thermal test because temperature profiles are available for both the shroud and O-ring/flange regions. Initially, only the values of the ambient heat transfer coefficients, h_a and h_b in Eqs. (3) and (4), are modified. A trial and error method is used to obtain the best match between the model prediction and the experimentally observed temperatures. The best predictions obtained by modifying only the heat transfer coefficients are shown in Figure 4. Here, the model predicts that the shroud cools off much more rapidly than what is observed experimentally. Additionally, the

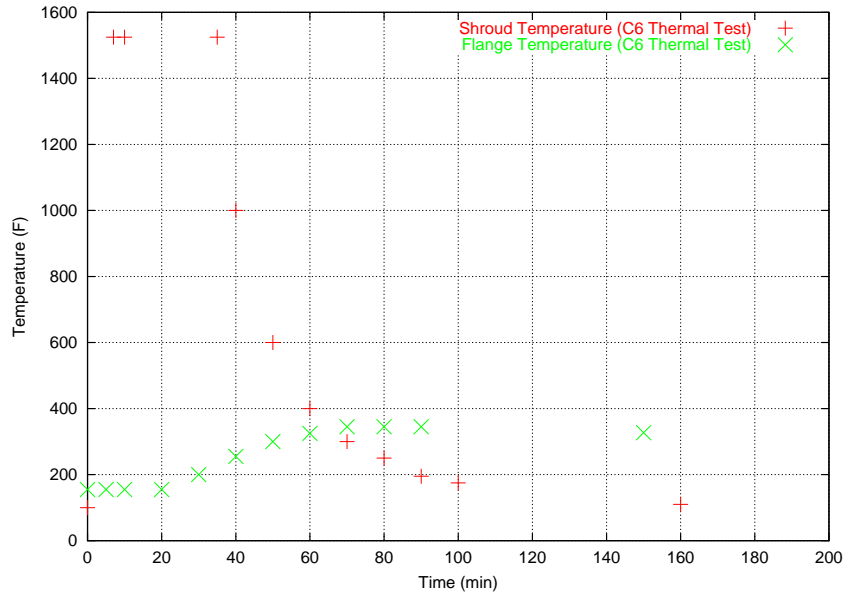


Figure 2. Experimentally Observed Temperature Histories during the C6 Thermal Test.

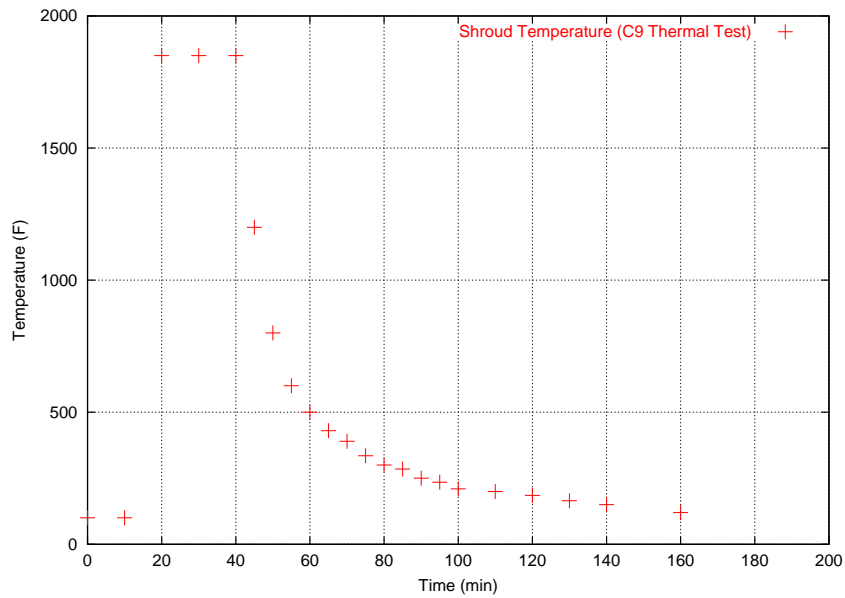


Figure 3. Experimentally Observed Temperature History during the C9 Thermal Test.

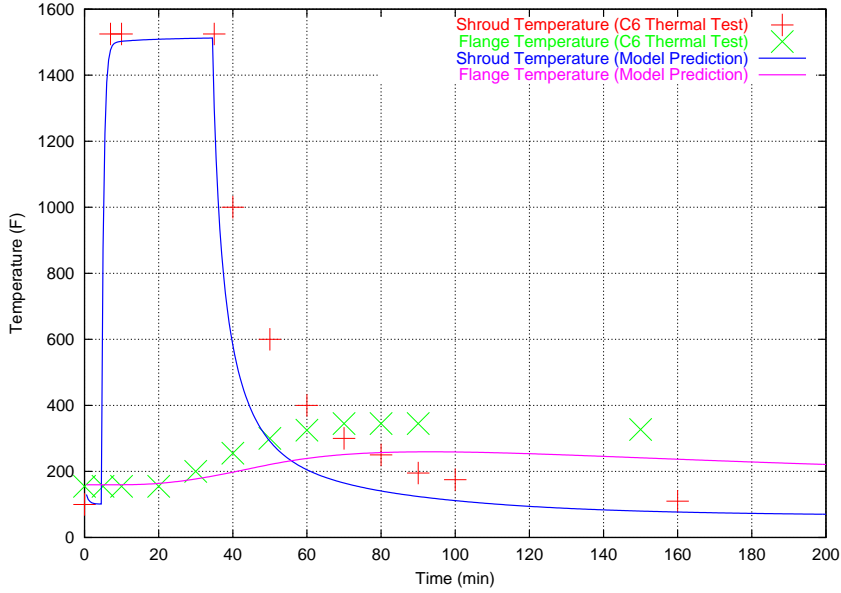


Figure 4. Calibration to the C6 Thermal Test using only the Heat Transfer Coefficients.

predicted maximum flange temperature is approximately 270°F, significantly less than the observed value of 344.7°F.

It was determined that in order for the predicted profiles to match the experimentally observed values, an additional heat generation source is required within the system. After additional discussions with several people who observed the thermal test, it is determined that at the conclusion of the thermal experiments, the polyurethane foam surrounding the inner containment vessel is typically burning. It is observed that the foam first expands and then contracts so that it effectively disintegrates into a small amount of material at the bottom of the shipping container. This observation supports the idea that temperatures reached within the polyurethane foam layer are high enough to catch the foam on fire during the heating portion of the experiment. The heat released during this process serves as an additional heat source. In addition, the thermal properties of the foam may change substantially after being burned. If the foam completely decomposes within the container, it may also be necessary to allow for thermal radiation across this newly formed air interface. However, for the present analysis, the foam is assumed not to disintegrate and form a void space. Additionally, brief experimentation with the thermal properties of the foam during the fire shows no significant change to the predicted temperatures. Consequently, the thermal properties of the foam as a function of temperature are not modified after the foam fire. While it would be beneficial to investigate the manner in which the foam burns

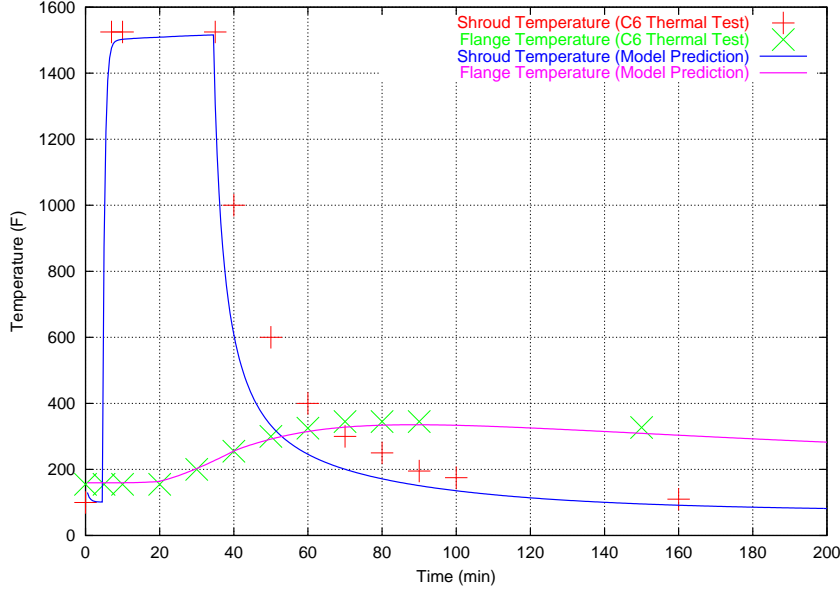


Figure 5. Calibration to the C6 Thermal Test including Foam Fire Effects.

and how its properties are modified because of the fire, the urgency of the final results require that crude assumptions be made on the effects of the internal polyurethane fire on the thermal response of the shipping container. In the approach taken, the burning foam is included as an energy source that heats the system between designated start and end times which are determined by trial and error. In future studies it would be beneficial to determine the temperature at which the foam starts to burn and associate the start of the foam fire with the time this temperature is reached.

The amount of heat generated by the foam fire is determined by multiplying the total heat of combustion, H_c (7.22 MJ/kg [1]), by the density, ρ_f of the polyurethane foam. This yields the number of Joules released per volume if the foam burns completely. To take into account incomplete combustion, a parameter known as the *fire factor*, χ , is introduced. This factor may be interpreted as the percentage of the foam that burns in the time between a specified fire start and end time. The total number of Watts generated per volume during the foam fire is then given as:

$$q_{foam} = \chi \frac{H_c \rho_f}{t_e - t_s}, \quad (5)$$

where the fire factor, χ , and fire start and end times, t_s and t_e , are additional parameters to be estimated.

The results of calibrating the numerical model using these additional parameters are

shown in Figure 5 using the parameters specified in Table 7. The predicted flange temperatures are now found to be considerably closer to the experimentally observed values than the previous predictions made without considering the foam fire. The maximum flange temperature is estimated to be 335.5°F which is much closer to the observed value of 344.7°F than the 270°F value determined earlier. However, while the predicted shroud temperatures are closer to the observed values, there is not a suitable match. The effects of the foam fire are seen to more directly affect the temperature at the flange than the temperature at the shroud. This is expected since the flange is physically closer to the foam fire, being separated only by a stainless steel layer which has a high thermal conductivity.

The predicted shroud temperature is found to be most sensitive to the emissivity value used for the outer steel drum. The best match between predicted and observed values of both the flange temperature and shroud temperature profiles is obtained when it is assumed that the emissivity of the outer steel container changes after the fire. An emissivity factor that is 20% of the tabulated value gives the best match to experimental data. This value is considerably smaller than expected. After completing the analysis, it is determined that the shroud is not the outer skin of the shipping container as assumed. Instead, the shroud is a large metal plate that surrounds the shipping containers during the thermal tests. A sample experimental layout is shown in Figure 6. The radiant heat lamps are focused on these stainless steel metal shrouds to more evenly distribute the energy to the shipping containers. The thermal model does not explicitly take into account the relationship between the metal shroud, the shipping container, and the air between them. Instead, it is assumed that the determined emissivity value is actually an effective property that implicitly takes into account these effects. Although this practice is not standard and leads to an uncharacteristic emissivity, it is not anticipated that it will impact the conclusions of the current analysis as we are primarily concerned with the the temperature history at the O-ring and flange which lie within the container.

The temperature history resulting from the final calibration to the C6 thermal experiment is shown in Figure 7. The maximum flange temperature of 345°F is essentially the same as the observed value of 344.7°F. During the calibration of the model with the thermal tests, no solar flux effects are included since initial tests indicated that the addition of a solar flux effects results in temperatures much higher than those observed during the experiment. It is concluded that there are minimal effects due to solar heat flux during the actual thermal experiments.

Once the model is successfully calibrated using the data from the C6 thermal test, it is desired to use the same model parameters to match the C9 thermal test data. Although using the parameters determined from the C6 thermal test yield a qualitative match of the temperature history to the C9 data, it is necessary to make additional modifications to obtain a satisfactory match. The parameters determined in the C9 calibration are shown in Table 7 and the comparison to the thermal experiment is shown in Figure 8. The maximum flange temperature reached is 465.7°F which corresponds closely to the observed value of 465°F. The most substantial change between the parameters when calibrating using the two

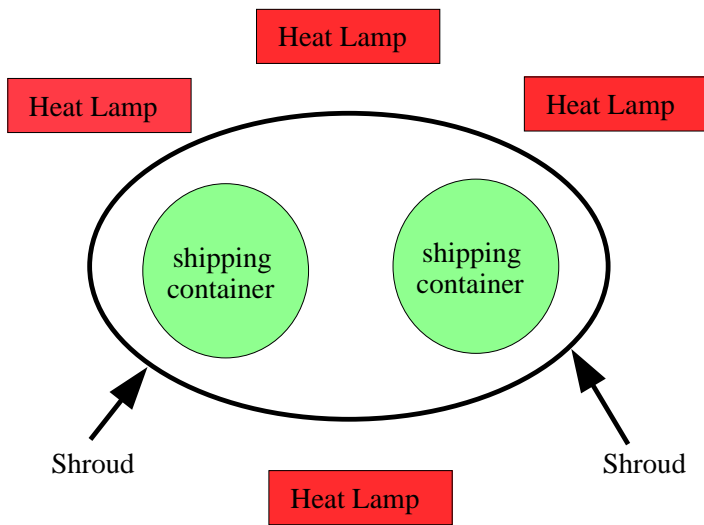


Figure 6. Shipping Container and Shroud Placement during Thermal Tests.

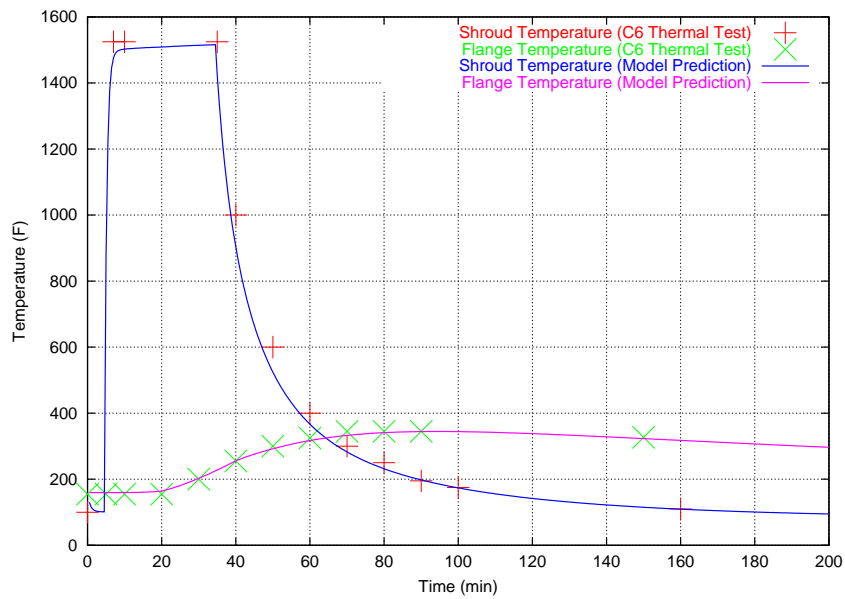


Figure 7. Final Calibration Results using the C6 Thermal Test Data.

Table 7. Final Model Parameters determined through Calibration.

	C6 Thermal Test	C9 Thermal Test
Foam Fire Start (t_s)	20 minutes	30 minutes
Foam Fire End (t_e)	40 minutes	50 minutes
Foam Fire Factor (χ)	0.14	0.32
Heat Transfer Coefficient (h_b)	5.5 W/m ² °K	7.0 W/m ² °K
Emissivity (% of tabulated) (ϵ)	0.20	0.20
Cooling Air Temp	40° F	40° F

Table 8. System Properties Predicted from Thermal Calibration Tests.

	C6 Test	C9 Test
Foam Fire Duration	20 minutes	20 minutes
Foam Fire Heat Generation	117,628 W/m ³	260,460 W/m ³
Max. Flange Temp. (Predicted)	345.0° F	465.7° F
Max. Flange Temp. (Experimental)	344.7° F	465.0° F

thermal experiments is seen in fire factor, χ . The fire factor determined in the C9 thermal test is 0.32, a value larger than the value of 0.14 determined in the C6 thermal test. This implies that the foam released more energy in the C9 test which may be a consequence of the higher temperature reached by the polyurethane foam layer due to the higher shroud temperature.

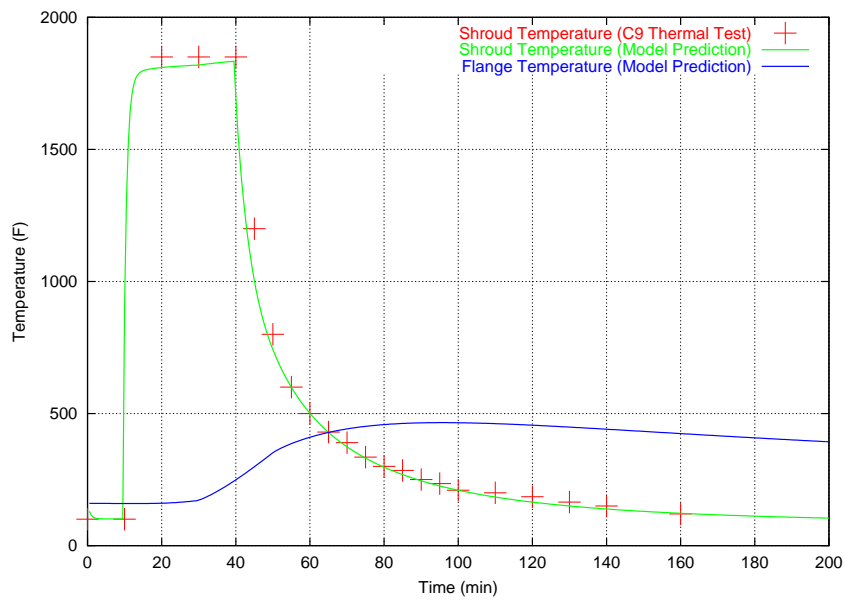


Figure 8. Final Calibration Results using the C9 Thermal Test Data.

4 Analysis and Results

Once the model is calibrated using the experimental thermal tests, it is possible to simulate the thermal tests and evaluate several different scenarios. In the following sections, temperature histories associated with each scenario are determined and are compared with a simulation of the C9 thermal test. The first section simulates the thermal response of a pre-heated shipping container and compares it with a simulation that explicitly models a heat source in the center of the shipping container. The second section describes simulations of the thermal tests at the ambient conditions specified by the Federal documents. The last section describes simulations of thermal tests at the ambient conditions specified by the Federal documents and which include the effects of solar insolation. A summary of the thermal conditions used in each of the scenarios is shown in Table 9.

Simulation of Thermal Tests including an Internal Heat Source

Thermal testing of the H1616 shipping containers is necessary to demonstrate that the containers are able to satisfactorily withstand thermal environments that may be present during accident conditions. The containers are designed to transport a radioactive material which may continuously generate a maximum of 6.5 Watts. Because of the dangers associated with handling radioactive materials, it is not possible to test filled containers. Thus, the elevated temperature distribution within a filled container, which is due to the presence of the radioactive material, is taken into account thermally by pre-heating empty shipping containers to an elevated temperature. This pre-heat temperature is typically chosen to be greater than the highest expected temperature found in a filled container at steady-state conditions. While this technique adequately takes into account the higher initial condition, it does not simulate the generation of heat throughout the entire thermal tests. Thus the effectiveness of the technique diminishes as the test proceeds. One question to be answered by this analysis is whether the maximum O-ring/flange temperature measured using the pre-heating technique provides a conservatively high measure of the maximum O-ring/flange temperature that would be observed in a filled shipping container.

In order to evaluate the pre-heating technique, the C9 thermal test is first simulated as performed in the field. The results of this simulation serve as a point of reference with which to compare additional simulations. This simulation, which is labeled the C9SIM scenario, involves first pre-heating an empty shipping container in a 160°F environment until thermal equilibrium is established. The container is then exposed to a powerful heat source which quickly brings the outside temperature of the shipping container to 1825°F. After thirty minutes of exposure, the powerful heat source is removed and the container is allowed to cool in a 40°F environment. After the C9 thermal test has been simulated, the determined temperatures are compared with temperatures determined in additional simulations that take into account a number of different conditions. In this manner, it is

possible to evaluate the thermal effects of including an internal heat source, increasing the ambient cooling temperature, and/or taking into account solar insolation. The ability for the C9 thermal test to predict a conservatively high maximum flange temperature for each of the various scenarios is determined by ensuring that the maximum flange temperature measured in the C9 thermal test is greater than the maximum flange temperature predicted in the remaining scenarios.

The first group of scenarios to be simulated repeat the C9 thermal test without the pre-heating step and include the effects of an internal heat source. Before this heat source can be simulated, it is necessary to determine a suitable value for the heat flux to be applied to the interior of the shipping container. The reservoir that contains the heat source releases a maximum of 6.5 W. It is approximately spherical and is located at the center of the shipping container. Because each of the layers in the shipping container is modeled as a cylinder, it is necessary to convert the heat source into an appropriate flux. There are two possible approaches. The first determines the heat flux across the surface area of the reservoir sphere and then uses the same value over the surface of a cylinder. This provides a worst case situation and results in a heat flux of $356.33 \text{ W}/m^2$. Over a cylinder of length one meter, this corresponds to 85.3 W, a value much larger than the spherical value of 6.5 Watts. Simulating the C9 thermal test using this value results in temperatures much higher than expected. A second approach that determines the heat flux required for a one meter cylinder to produce 6.5 Watts yields a value of $27.15 \text{ W}/m^2$.

The most appropriate value for the heat source is determined by simulating a steady-state thermal experiment that was conducted using resistance heating for the original SARP report [6]. Here a shipping container with a 6.5 Watt heat source is allowed to come to thermal equilibrium in a 100°F environment. The maximum observed temperature during the experiment is 148°F which is reached at the center reservoir. The developed model is used to simulate this steady-state thermal experiment and determine the temperature distributions associated with three different heat flux values, $27.15 \text{ W}/m^2$, $60 \text{ W}/m^2$, and $120 \text{ W}/m^2$. Figure 9 shows the determined steady-state temperature profiles as a function of radial position. The temperature distribution is axisymmetric and the x-axis indicates the distance from the center of the shipping container. For each flux, the highest temperature is predicted at the reservoir (around 0.04 meters). The temperature variations as a function of position seen in Figure 9 are due to the various materials that comprise the shipping container. The area of interest, the location of the flange and O-ring, is located at approximately 0.157 meters from the center of the container. Based on the results of the simulations, a heat flux of $80 \text{ W}/m^2$ is seen to provide a maximum temperature of 150°F which is suitably close to the observed value of 148°F . Using this flux, the predicted O-ring/flange temperature at steady-state is approximately 128°F which is 28°F greater than the ambient temperature. In addition to evaluating the $80 \text{ W}/m^2$ flux, a conservatively high value of $120 \text{ W}/m^2$ is also examined.

The developed model is now used to estimate the temperature history of a filled container. The influence of the radioactive material at the center of the shipping container is

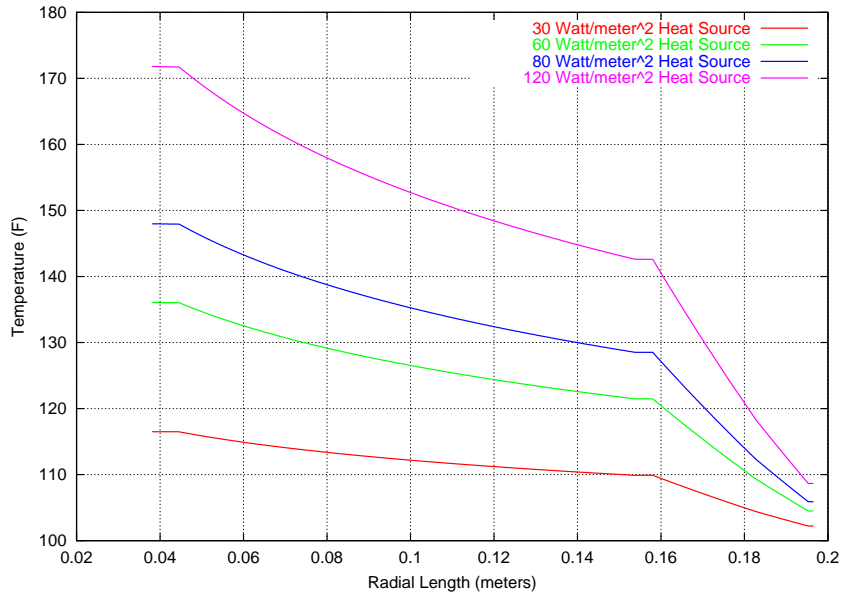


Figure 9. Steady-State Temperature Profiles for Different Values of Internal Heat Flux.

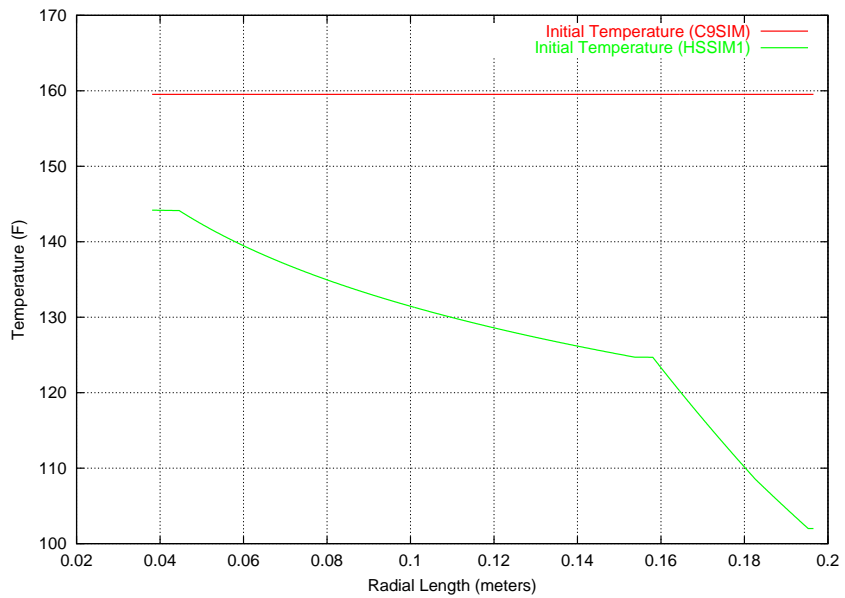


Figure 10. Initial Steady-State Temperature Distribution (C9SIM vs. HSSIM1).

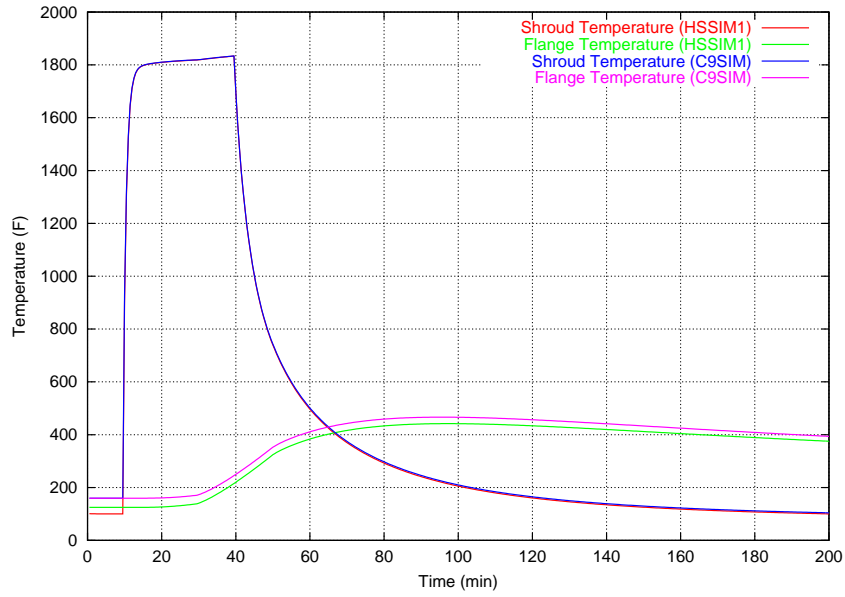


Figure 11. Temperature Histories for Simulated Thermal Tests (C9SIM vs. HSSIM1).

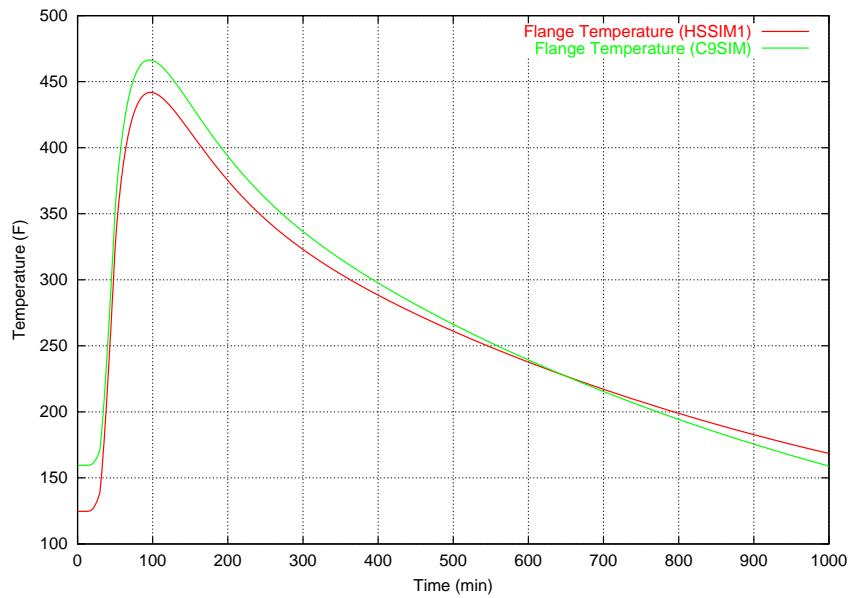


Figure 12. Flange Temperatures for Simulated Thermal Tests (C9SIM vs. HSSIM1).

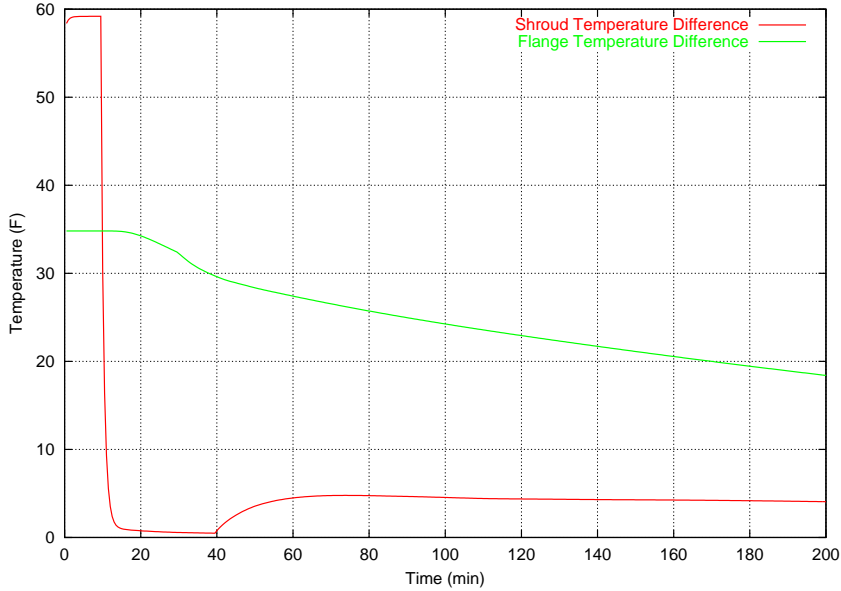


Figure 13. Temperature Differences for Simulated Thermal Tests (C9SIM vs. HSSIM1).

simulated as an internal heat source that generates a flux of $80 \text{ W}/m^2$ flux on the inner reservoir boundary. This scenario is labeled the HSSIM1 scenario to indicate it is the first scenario where the Heat Source is simulated. One of the key differences between the C9SIM scenario and the scenarios where the heat source is explicitly modeled is in the profile of the initial temperature conditions. Pre-heating the shipping container results in an elevated uniform temperature distribution while simulation of the heat source provides a temperature distribution within the shipping container. The initial steady-state temperatures reached before exposure to the intense heating source for both the C9SIM and HSSIM1 are shown in Figure 10. It is seen that the C9SIM temperature provides a conservatively high estimate of the temperature distribution in the HSSIM1 scenario over the entire container.

The shroud and flange temperature histories for the complete C9SIM and HSSIM1 scenarios are shown in Figure 11. While the shroud temperatures predicted in both scenarios are very similar, the flange temperature in the C9SIM scenario overpredicts the flange temperature observed in the HSSIM1 scenario. The maximum flange temperature predicted in the HSSIM1 scenario is 441.90°F which is less than the 466.40°F predicted in the C9SIM scenario. However, the ability of the C9SIM scenario to overpredict the expected flange temperature decreases as the thermal test proceeds. This is seen in Figure 12 which compares the flange temperatures over a much longer period of time. The time at which the flange temperature predicted by the C9SIM falls below the flange temperature estimated for

a particular scenario is defined as the *cross over* point. For the HSSIM1 scenario the cross over point occurs at approximately 650 minutes. After this time, the C9SIM scenario, which simulates the pre-heating technique, no longer provides a conservatively high estimate of the actual flange temperature. Fortunately, the time at which the flange reaches its maximum temperature is around 90 minutes, so that the C9SIM scenario provides a conservative estimate of this maximum value. The temperature difference between the two scenarios is plotted in Figure 13 for both the shroud and flange temperatures. A positive value indicates that the temperatures in the C9SIM scenario are greater than those in the HSSIM1 scenario. At the time of the maximum flange temperature (90 minutes), the difference in flange temperature between the two scenarios is 24.5°F

In order to ensure a conservatively high heat flux is evaluated, a second scenario is evaluated that uses a 120 W/m² heat flux to simulate the internal heat source. The initial steady-state temperatures for both the C9SIM and HSSIM2 scenarios are shown in Figure 14. It is seen that the C9SIM temperature provides a conservatively high estimate of the temperature distribution in the HSSIM1 scenario over only a portion of the shipping container. At the O-ring/flange location however, the C9SIM scenario still predicts a conservatively high temperature. The shroud and flange temperature histories for the complete C9SIM and HSSIM2 scenarios are shown in Figure 15. Again the shroud temperatures predicted in both scenarios are very similar. The maximum flange temperature predicted in the HSSIM2 scenario is 452.86°F. This is greater than the 441.90°F temperature observed in the HSSIM1 scenario, but is still less than the 466.40°F predicted in C9SIM. Figure 16 compares the flange temperatures over a much longer period of time. The cross over point for the HSSIM2 scenario is at 230 minutes, which is more than half of the time observed in the HSSIM1 scenario. This indicates that the C9SIM provides a conservative estimate for a considerably shorter time, but still suitably overpredicts the maximum flange temperature. The temperature difference between the two scenarios is plotted in Figure 17 for both the shroud and flange temperatures. The difference in maximum flange temperature predicted by the two scenarios is 13.54°F

Simulation of Thermal Tests at an Elevated Cooling Temperature

The analysis in the previous section indicates that the experimental technique of pre-heating an empty shipping container to simulate the internal heat source in a filled container provides a conservatively high measure of the maximum flange temperature for the actual conditions present during the C9 thermal test. The C9 thermal test is assumed to have occurred in a 40°F environment, which is characteristic of a cool day in New Mexico. However, Federal regulations require that compliance be shown in a 100°F environment. Using the developed model, the effects of cooling at an elevated temperature are evaluated for three different scenarios.

The first scenario, labeled CTSIM1 since it modifies the Cooling Temperature, repeats

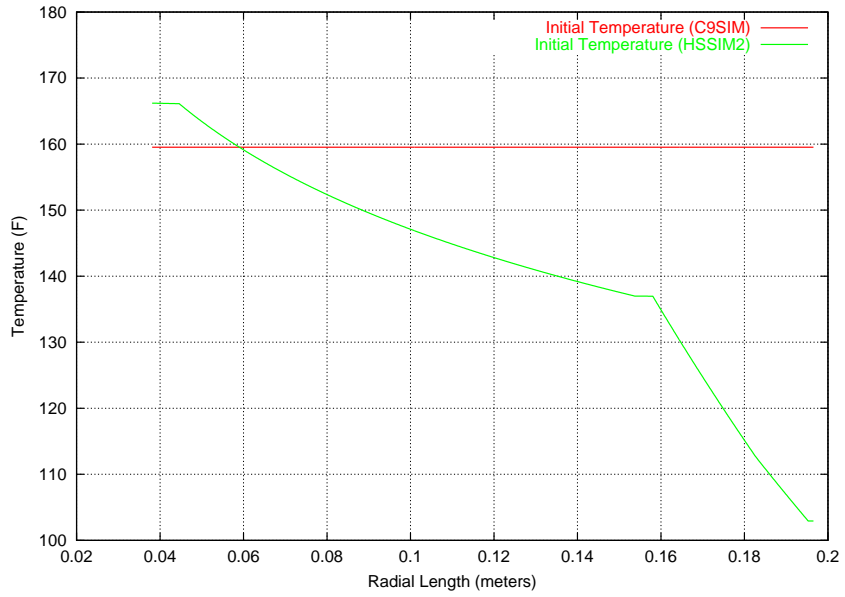


Figure 14. Initial Steady-State Temperature Distribution (C9SIM vs. HSSIM2).

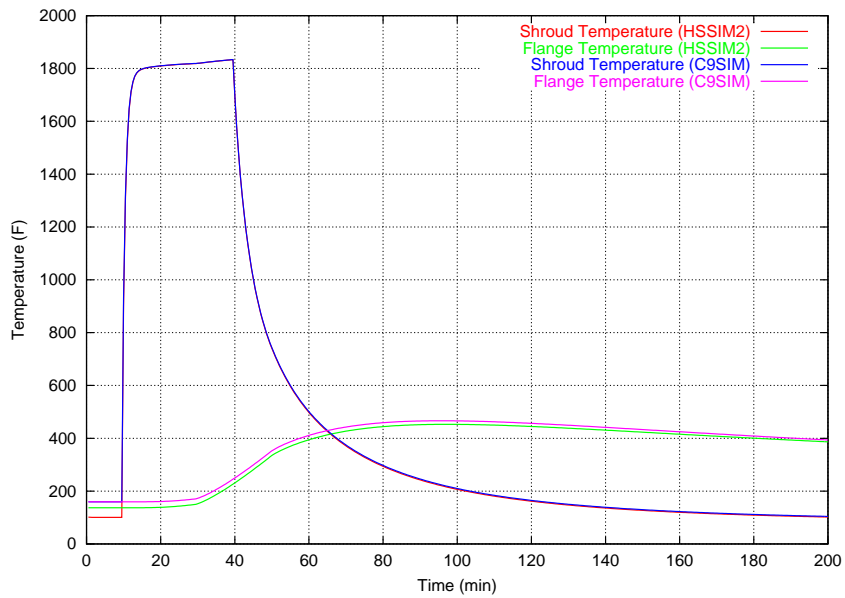


Figure 15. Temperature Histories for Simulated Thermal Tests (C9SIM vs. HSSIM2).

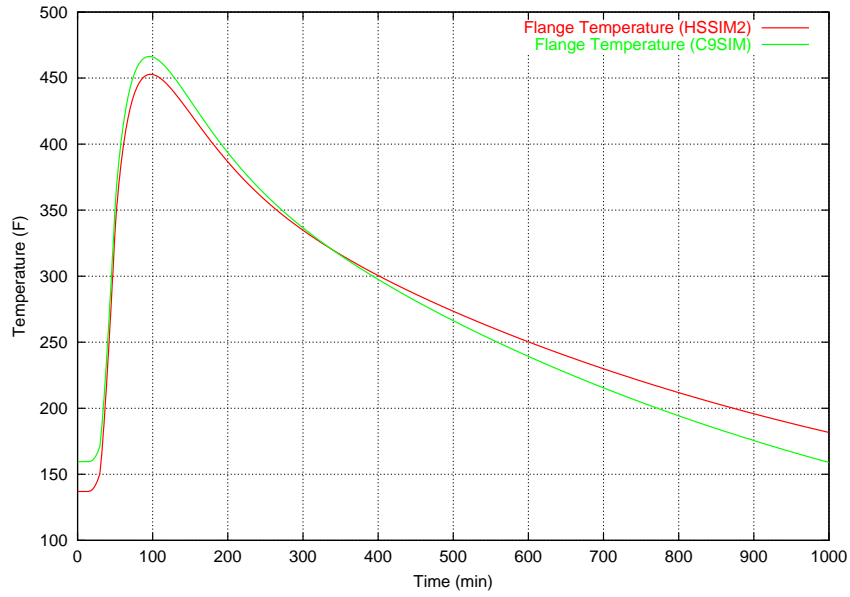


Figure 16. Flange Temperatures for Simulated Thermal Tests (C9SIM vs. HSSIM2).

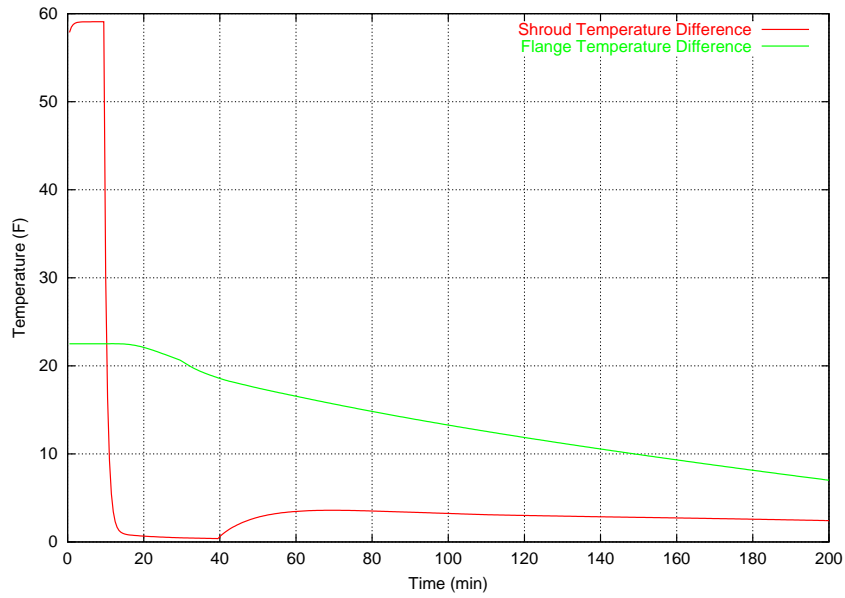


Figure 17. Temperature Differences for Simulated Thermal Tests (C9SIM vs. HSSIM2).

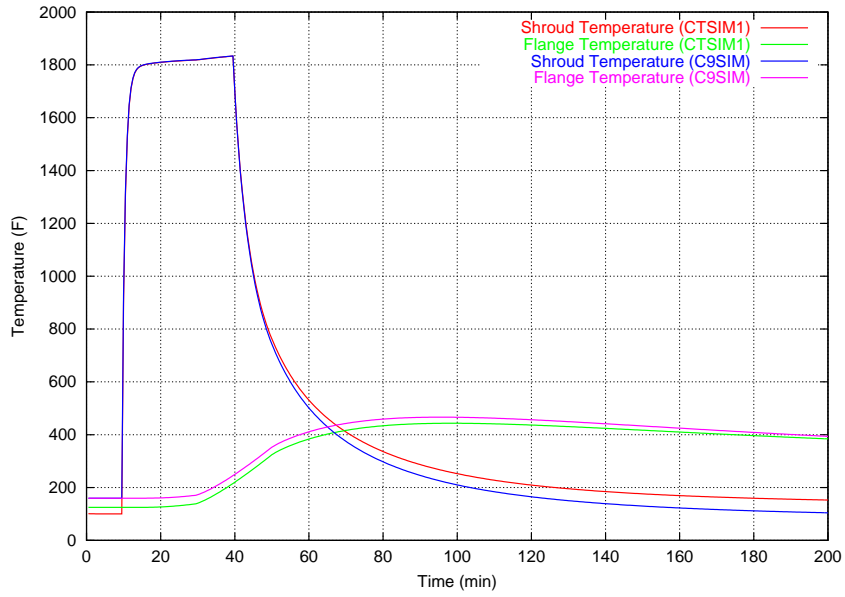


Figure 18. Temperature Histories for Simulated Thermal Tests (C9SIM vs. CTSIM1).

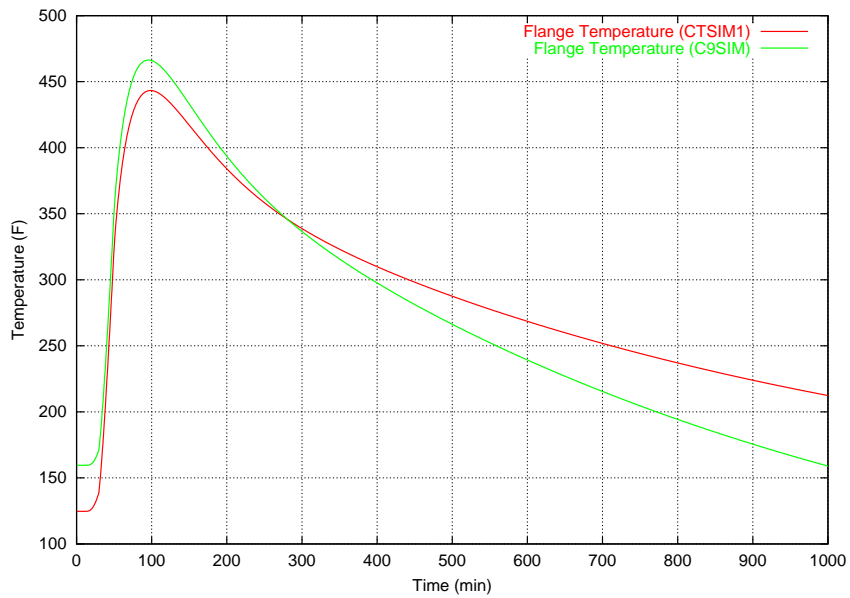


Figure 19. Flange Temperatures for Simulated Thermal Tests (C9SIM vs. CTSIM1).

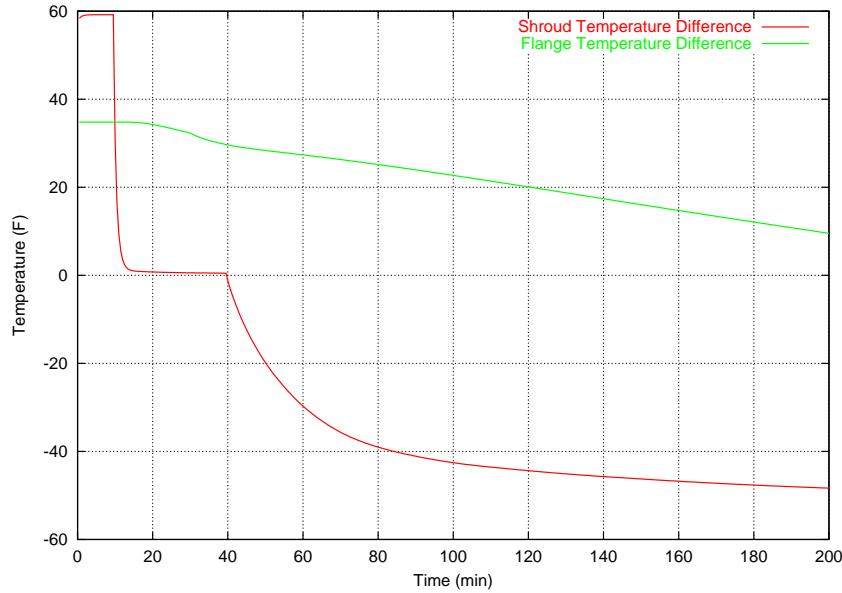


Figure 20. Temperature Differences for Simulated Thermal Tests (C9SIM vs. CTSIM1).

the HSSIM1 scenario at an ambient temperature of 100°F instead of 40°F . As in the HSSIM1 scenario, an internal heat source is modeled using a $80\text{ W}/\text{m}^2$ flux. The initial temperature profile for the CTSIM1 scenario is the same as for HSSIM1 and is shown in Figure 10. A comparison between the shroud and flange temperatures for the complete thermal test is shown in Figure 18. The maximum flange temperature predicted in the CTSIM1 scenario is 443.32°F which is 1.42°F greater than the 441.90°F predicted in the HSSIM1 scenario. Changing the ambient cooling temperature is seen to have a minimal effect on the maximum flange temperature, and the C9SIM scenario again overpredicts the flange temperature. The effects of changing the cooling temperature are seen most prevalent in the cooling portion of the thermal test where the temperature levels out at the new cooling temperature of 100°F instead of 40°F . Figure 19 provides a longer look at the thermal simulation and shows the cross over point to be at approximately 275 minutes. The temperature difference between the two scenarios is plotted in Figure 20 for both the shroud and flange temperatures. At the time of the maximum flange temperature (90 minutes), the temperature difference between the C9SIM and CTSIM1 scenarios is 23.08°F .

A second scenario, known as CTSIM2, is simulated to evaluate the effects of cooling at 120°F , a conservatively high temperature. As with the CTSIM1 scenario, this scenario repeats the HSSIM1 scenario, but at an ambient temperature of 120°F . A $80\text{ W}/\text{m}^2$ flux is used to model an internal heat source and the initial temperature profile is again the same as

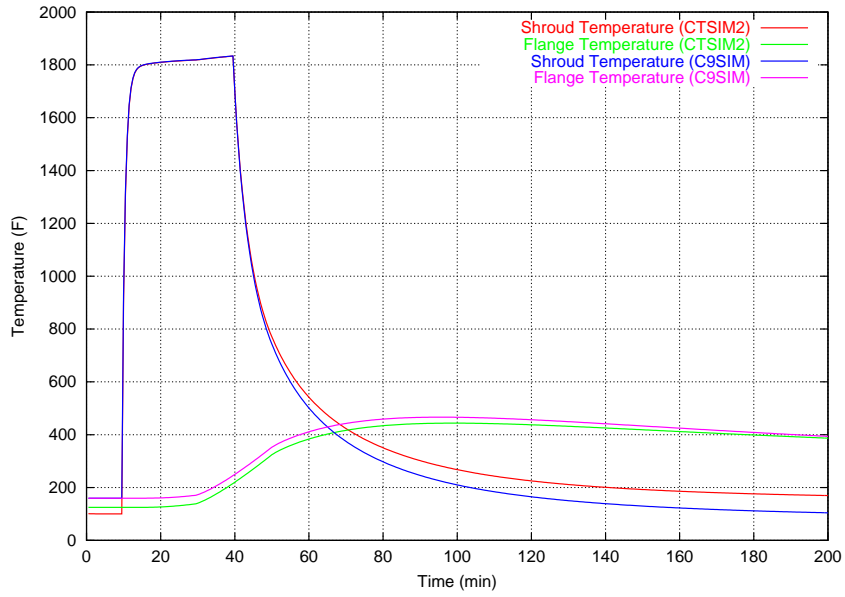


Figure 21. Temperature Histories for Simulated Thermal Tests (C9SIM vs. CTSIM2).

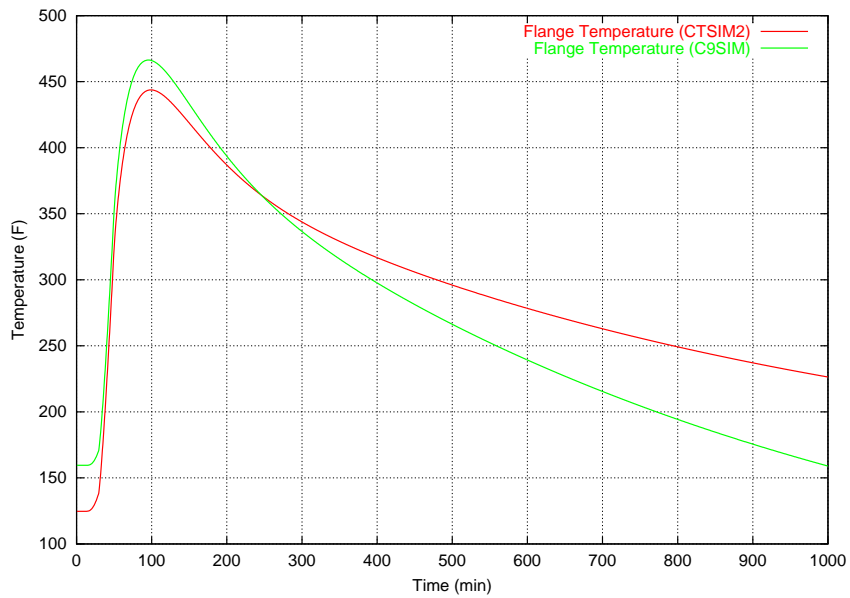


Figure 22. Flange Temperatures for Simulated Thermal Tests (C9SIM vs. CTSIM2).

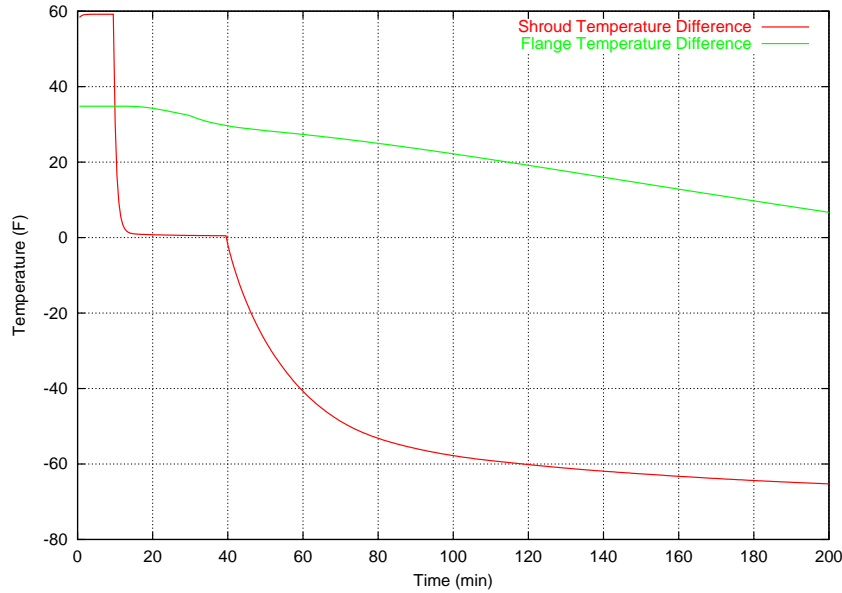


Figure 23. Temperature Differences for Simulated Thermal Tests (C9SIM vs. CTSIM2).

for the HSSIM1 scenario. A comparison between the shroud and flange temperatures for the complete thermal test is shown in Figure 21. The maximum flange temperature predicted in the CTSIM2 scenario is 443.80°F which is 1.9°F greater than the 441.90°F predicted in the HSSIM1 scenario. This re-iterates the point that the ambient cooling temperature has a minimal effect on the maximum flange temperature. Figure 22 provides a longer look at the thermal simulation and shows the cross over point to be at approximately 250 minutes. The temperature difference between the two scenarios is plotted in Figure 23 for both the shroud and flange temperatures. At the time of the maximum flange temperature, the difference between the C9SIM and CTSIM2 scenarios is 22.60°F.

A third scenario is defined to evaluate the most unfavorable conditions examined to this point. The CTSIM3 scenario examines the effects of using conservatively high values for both the heat source flux, 120 W/m², and an ambient cooling temperature, 120°F. The initial temperature profile is the same as for the HSSIM2 scenario which is shown in Figure 14. A comparison between the shroud and flange temperatures for the complete thermal test is shown in Figure 24. The maximum flange temperature predicted in the CTSIM2 scenario is 454.77°F which is 1.9°F greater than the 452.86°F predicted in the HSSIM2 scenario. This is the same temperature difference seen between the HSSIM1 and CTSIM2 scenarios. Figure 25 provides a longer look at the thermal simulation and shows the cross over point to be at approximately 168 minutes. The difference between the two scenarios

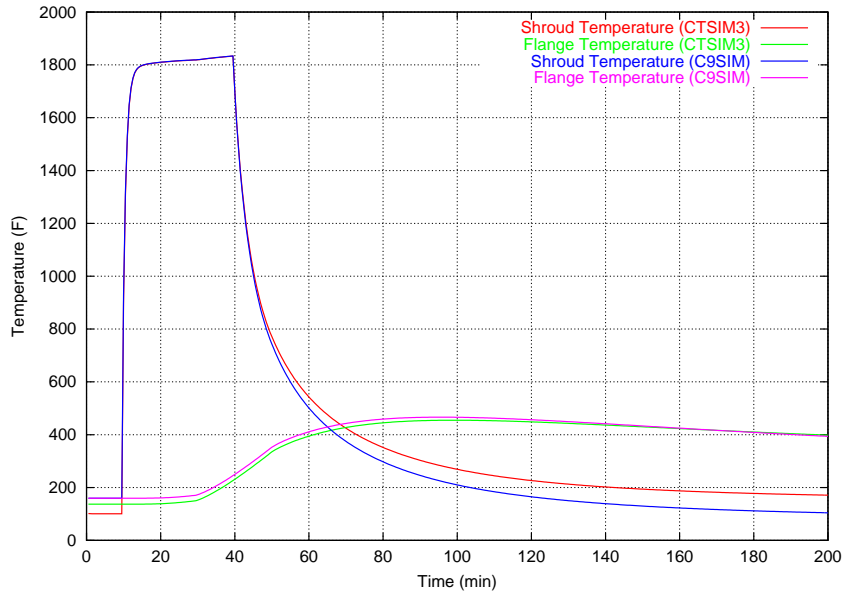


Figure 24. Temperature Histories for Simulated Thermal Tests (C9SIM vs. CTSIM3).

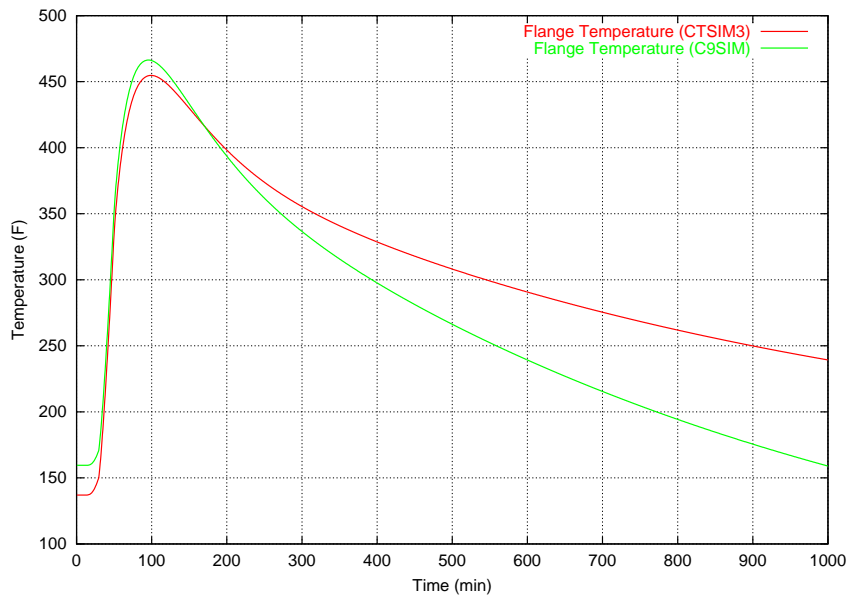


Figure 25. Flange Temperatures for Simulated Thermal Tests (C9SIM vs. CTSIM3).

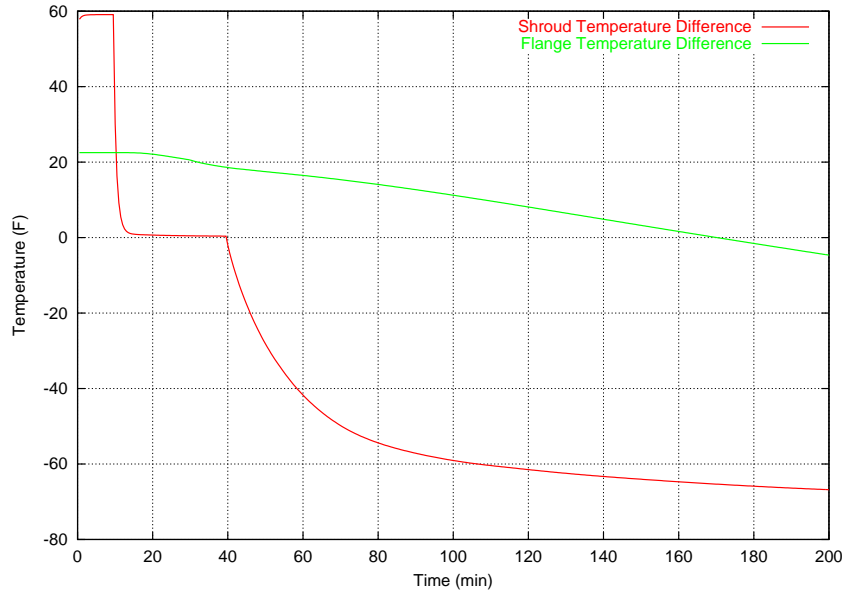


Figure 26. Temperature Differences for Simulated Thermal Tests (C9SIM vs. CTSIM3).

is plotted in Figure 26 for both the shroud and flange temperatures. At the time of the maximum flange temperature, the temperature difference between the C9SIM and CTSIM3 scenarios is 11.63°F.

Simulation of Thermal Tests undergoing Solar Insolation

In addition to requiring an ambient cooling temperature of 100°F, Federal regulations also specify that compliance must be shown for exposure to a constant solar heat flux for a twelve hour period following the cooling portion of the thermal tests. This is to be followed by twelve hours without insolation, at which time the cycle is repeated. The scenarios in this section model these additional effects by continuously applying a constant heat flux to the shipping container, i.e. not taking into account the cyclic process. This provides a conservatively high estimate of the thermal effects due to insolation. Before the solar insolation simulations are conducted, it is necessary to first determine an appropriate value for the observed heat flux. The value specified in the Federal document is 387.68 W/m² for curved surfaces. The observed flux is calculated by multiplying the solar insolation value by the solar absorptivity. For a typical stainless steel, the solar absorptivity is 0.37, which leads to an observed flux of 143.44 W/m².

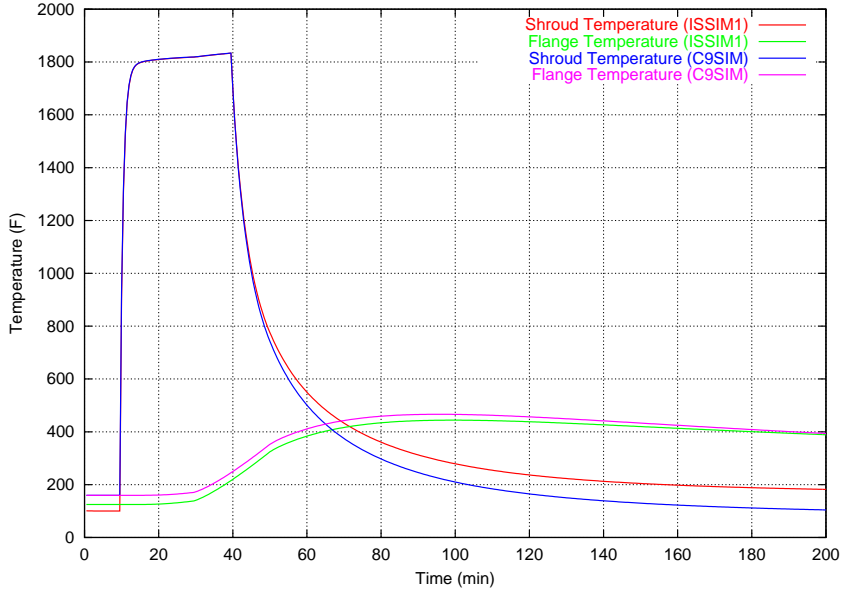


Figure 27. Temperature Histories for Simulated Thermal Tests (C9SIM vs. ISSIM1).

The first scenario exploring the effects of solar InSolation is labeled, ISSIM1. In this scenario, the CTSIM1 scenario is repeated using a solar flux of 143.44 W/m^2 . The initial steady-state temperatures profile reached before exposure to the intense heating source is the same as the CTSIM1 scenario. A comparison between the shroud and flange temperatures for the complete thermal test is shown in Figure 27. The maximum flange temperature predicted in the ISSIM1 scenario is 444.16°F which is 0.84°F greater than the 443.32°F predicted in the CTSIM1 scenario. As with the ambient cooling temperature, solar insolation effects are seen to have a minimal impact on the maximum flange temperature. The C9SIM scenario is able to give a conservatively high value for the maximum flange temperature. Figure 28 provides a longer look at the thermal simulation and shows the cross over point to be at approximately 235 minutes. The effects of including solar insolation are seen in the final temperature reached toward the end of the thermal test. The temperature difference between the two scenarios is plotted in Figure 29 for both the shroud and flange temperatures. At the time of the maximum flange temperature, the difference between the C9SIM and ISSIM1 scenarios is 22.24°F .

A conservatively high value of the insolation effects is evaluated in a second scenario. This scenario is labeled ISSIM2 and is similar to the CTSIM1 scenario with the exception that a solar flux of 300 W/m^2 , a value approximately twice that of the value specified by the Federal regulations, is used. A comparison between the shroud and flange temperatures for

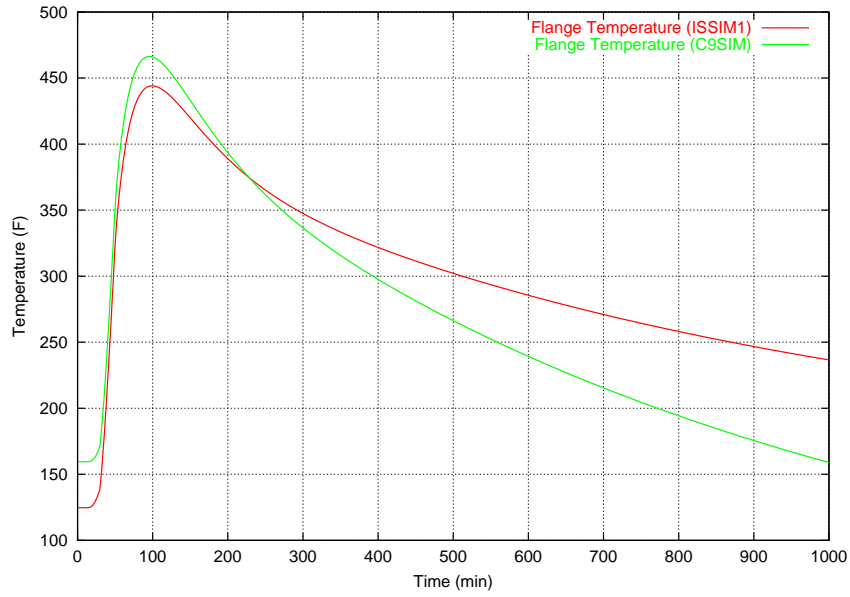


Figure 28. Flange Temperatures for Simulated Thermal Tests (C9SIM vs. ISSIM1).

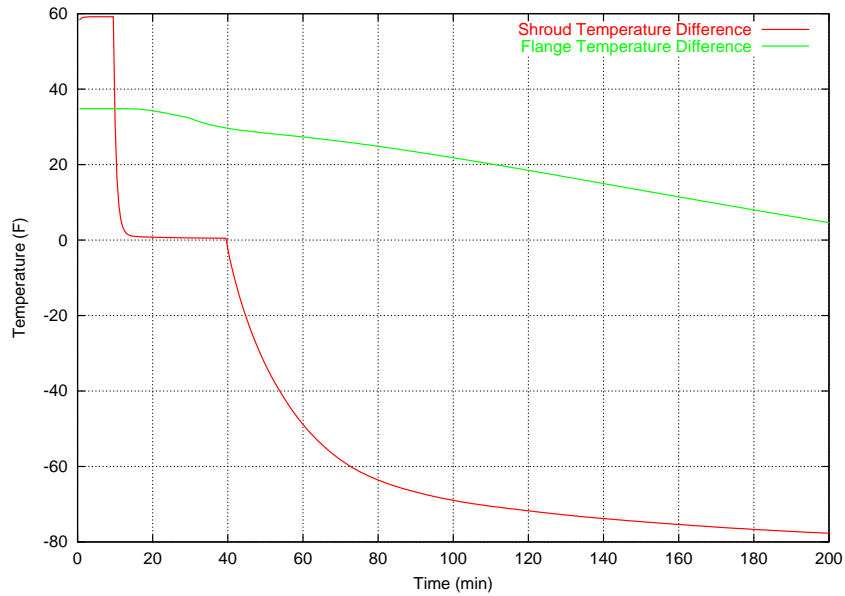


Figure 29. Temperature Differences for Simulated Thermal Tests (C9SIM vs. ISSIM1).

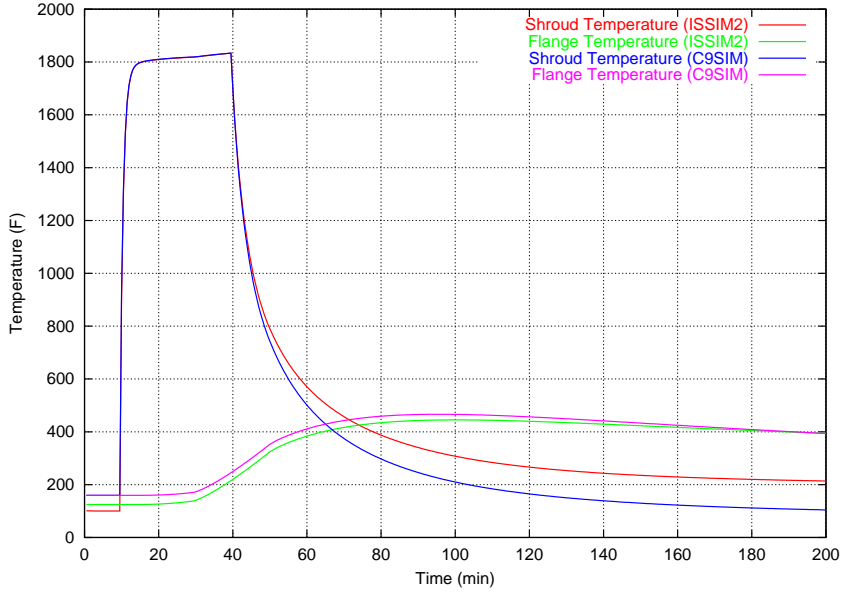


Figure 30. Temperature Histories for Simulated Thermal Tests (C9SIM vs. ISSIM2).

the complete thermal test is shown in Figure 30. The results are similar to those seen before. The maximum flange temperature predicted in the ISSIM2 scenario is 445.11°F which is 1.79°F greater than the 443.32°F predicted in the CTSIM1 scenario. Again, solar insolation effects have a minimal impact on the maximum flange temperature, and the C9SIM scenario is able to give a conservatively high value for the maximum flange temperature. Figure 31 provides a longer look at the thermal simulation and shows the cross over point to be at approximately 200 minutes. The difference between the C9SIM and ISSIM2 scenarios is plotted in Figure 32 for both the shroud and flange temperatures. At the time of the maximum flange temperature, the difference between the scenarios is 21.29°F .

Finally, a third scenario is defined to evaluate the most unfavorable conditions. This scenario is labeled ISSIM3 and evaluates the effects of including a $120\text{ W}/\text{m}^2$ heat source, cooling in a 120°F environment, and using the most extreme value of solar flux, $300\text{ W}/\text{m}^2$. A comparison between the shroud and flange temperatures for the complete thermal test is shown in Figure 33. For this scenario, the maximum predicted flange temperature is 456.59°F which is 9.81°F greater than the 466.40°F predicted in the C9SIM scenario. Figure 34 provides a longer look at the thermal simulation and shows the cross over point to be at approximately 140 minutes. This value is considerably shorter than previously seen but shows that even under the most unfavorable conditions, the C9SIM scenario is able to provide a conservatively high estimate of the maximum flange temperature. The temperature

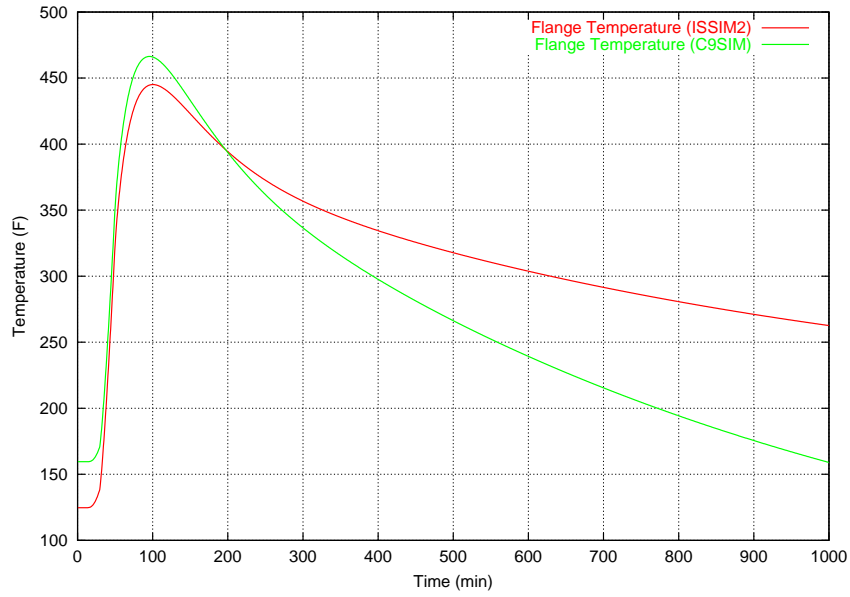


Figure 31. Flange Temperatures for Simulated Thermal Tests (C9SIM vs. ISSIM2).

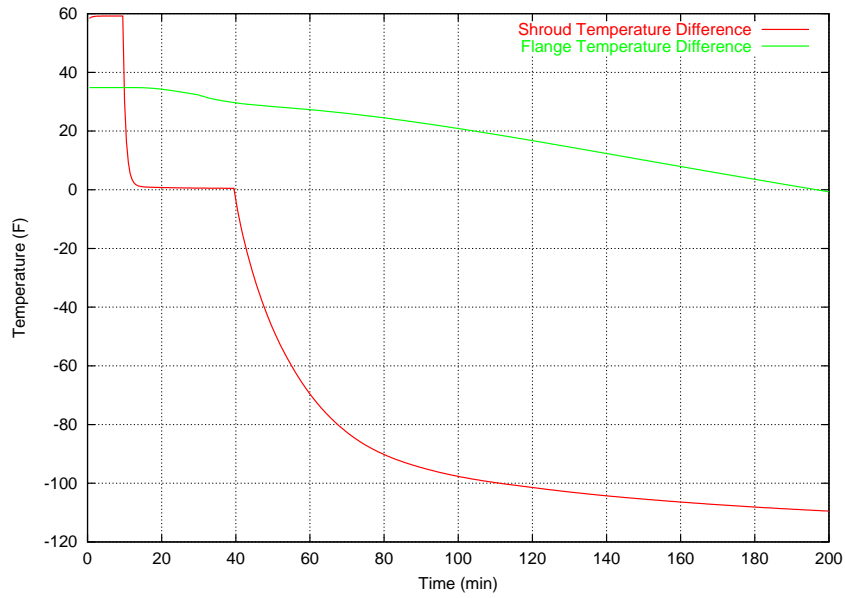


Figure 32. Temperature Differences for Simulated Thermal Tests (C9SIM vs. ISSIM2).

Table 9. Description and Results of the C9 Simulation Scenarios.

Scenario	Heat Source (W/m^2)	Cooling Temp. ($^{\circ}F$)	Insolation (W/m^2)	Max Flange Temp. ($^{\circ}F$)	Difference from C9SIM ($^{\circ}F$)	Cross Over (minutes)
C9SIM	–	40	–	466.40	–	00
HSSIM1	80	40	–	441.90	24.5	550
HSSIM2	120	40	–	452.86	13.54	230
CTSIM1	80	100	–	443.32	23.08	275
CTSIM2	120	120	–	443.80	22.60	265
CTSIM3	120	120	–	454.77	11.63	168
ISSIM1	80	100	143	444.16	22.24	235
ISSIM2	80	100	300	445.11	21.29	200
ISSIM3	120	120	300	456.59	9.81	140

difference between the C9SIM and ISSIM3 scenarios is plotted in Figure 35 for both the shroud and flange temperatures. The results of the solar insolation analysis are consistent with the results of a two-dimensional axisymmetric finite element analysis performed by Ohashi and Ortega(8727) [4].

The thermal conditions defining each of the scenarios and the maximum predicted flange temperature for each scenario are shown in Table 9. The table also reports the time at which the C9 thermal test is no longer able to adequately overestimate the flange temperature for each of the different scenarios, the cross over time. Since the cross over time for each of the scenarios is greater than the time the maximum flange temperature is reached (approximately 90 minutes), the C9 thermal test provides a conservatively high estimate of the maximum flange temperature in each scenario. This indicates that the pre-heating technique used in the various thermal tests is capable of taking into account the thermal effects present in a filled container. The results also show that as performed, the thermal tests provide a conservatively high estimate of the maximum flange temperature for several scenarios that meet or exceed the Federal regulations.

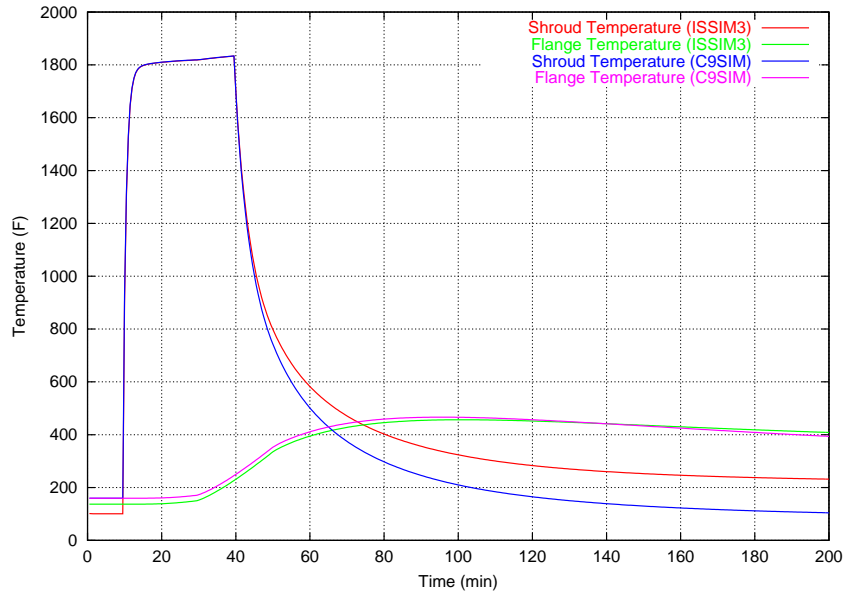


Figure 33. Temperature Histories for Simulated Thermal Tests (C9SIM vs. ISSIM3).

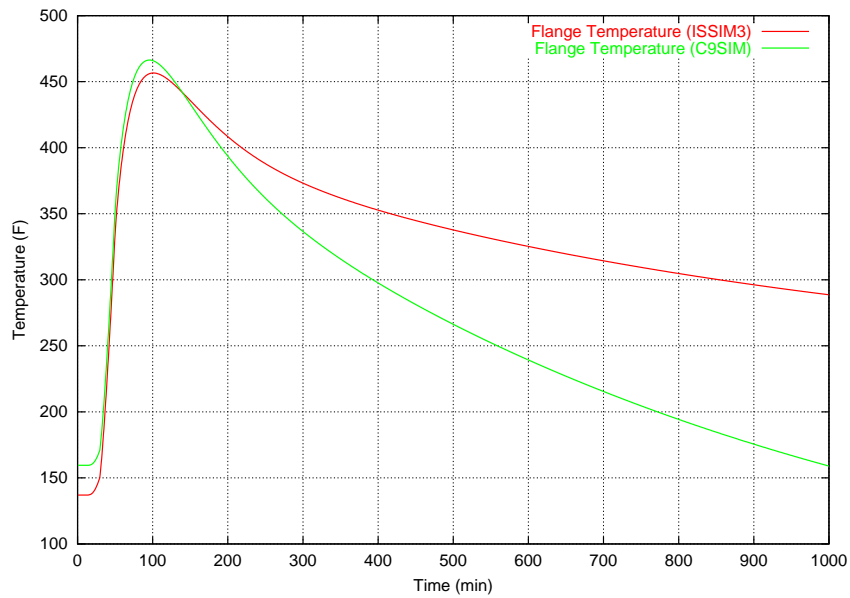


Figure 34. Flange Temperatures for Simulated Thermal Tests (C9SIM vs. ISSIM3).

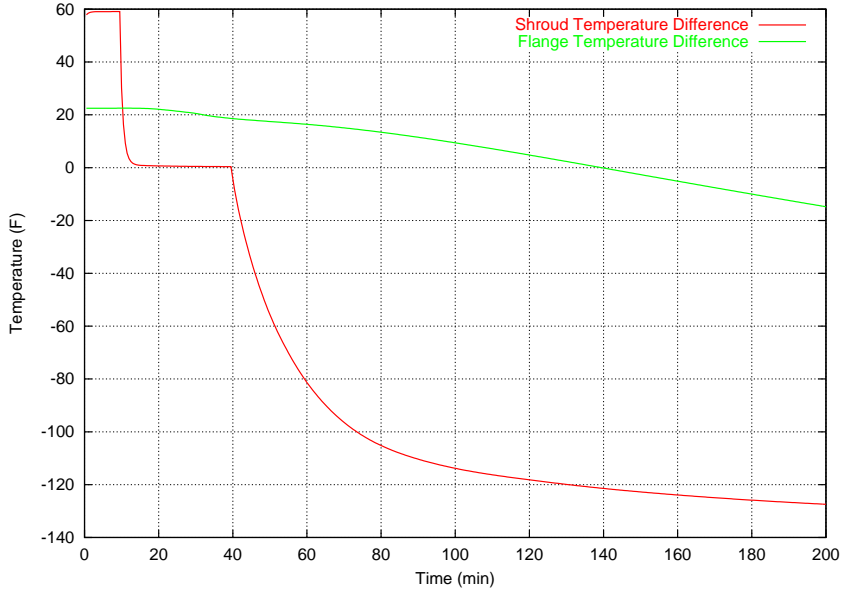


Figure 35. Temperature Differences for Simulated Thermal Tests (C9SIM vs. ISSIM3).

5 Conclusions

The goal of this analysis has been to show that the experimental thermal tests conducted for the certification of the H1616 shipping container provide a conservatively high estimate of the maximum flange temperature, a key measure of the thermal response of the shipping container. During the thermal tests, dangers associated with the handling of radioactive material that normally would be prevalent in actual accident conditions were eliminated by simulating the effects of heat generation by pre-heating empty shipping containers to temperatures greater than those expected when using filled containers. Federal regulations also require cooling in a 100°F environment under a cyclic solar radiation load. In the actual thermal tests performed for certification, the cooling temperature was close to 40°F and no steps were taken to simulate solar insolation effects.

In order to show compliance with the Federal regulations, a computational model was developed to simulate the thermal response of the C9 thermal test as performed and for a number of different scenarios that met or exceeded the conditions specified by the Federal regulations. A one-dimensional finite difference model of the shipping container was developed in cylindrical coordinates. The model assumes the container is axisymmetric and allows for variable thermal properties in the radial direction. The model parameters were calibrated using shroud and flange temperature data obtained from two experimental

thermal tests. The calibrated model parameters led to physically realistic system properties.

Initial calibration steps predicted smaller than expected flange temperatures and it was determined that additional heat may be generated in the system by accounting for the heat released when the polyurethane foam layer catches on fire and releases some amount of energy. Calibration of the foam fire parameters indicated that the foam released energy for approximately twenty minutes. Because the reported shroud temperature were initially assumed to measure the skin temperature of a single shipping container, non-physical values of the emissivity of steel were determined during the calibration stage. The determined emissivity value therefore takes into account the thermal effects of the air between the shroud and each of the shipping containers and is interpreted as an effective property. This use is not expected to affect the results of this analysis.

Once calibrated, the model was used to evaluate the thermal response of the shipping container for several different scenarios. A first set of scenarios estimated the thermal response of a filled container by including a heat generation term into the model using a specified heat flux. Using a flux of $80\text{W}/\text{m}^2$ gave maximum steady-state temperatures that closely matched a steady-state thermal experiment conducted for the original SARP [6]. A conservatively high value of $120\text{W}/\text{m}^2$ was also evaluated. The magnitude of the heat generation source was seen to produce the largest changes to the observed maximum flange temperature. As the magnitude of the heat source term was increased, a shorter cross over time is determined and the temperatures estimated using the C9 thermal test become less an indicator of the true flange temperature. When using either the $80\text{W}/\text{m}^2$ and $120\text{W}/\text{m}^2$ heat flux for the heat source, pre-heating of empty shipping containers to 160°F adequately accounts for the effects of the heat generation source.

A second set of scenarios examined the impact of raising the temperature at which the shipping container is cooled. The original C9 thermal test was assumed to cool in a 40°F environment. Federal regulations require cooling in a 100°F environment. In these scenarios, an ambient temperature of 100°F was used in addition to a conservatively high temperature of 120°F . The results of the simulations showed that changes to the cooling environment temperature had a limited effect of on the maximum flange temperature. This is mainly a consequence of the fact that changes to the observed temperatures occur toward the end of the thermal experiment, well after the maximum flange temperature has been reached. A worst case scenario using a $120\text{W}/\text{m}^2$ heat flux and a 120°F cooling environment was also evaluated. For each case, the maximum flange temperature recorded in the C9 thermal test suitably overpredicted the maximum expected flange temperature.

A final set of scenarios were simulated to evaluate the impact of using two different solar fluxes. The simulations were conducted using an observed flux of $143.44\text{W}/\text{m}^2$, the flux set by Federal regulations for curved surfaces. A conservative solar flux of $300\text{W}/\text{m}^2$ is also evaluated. The resulting temperature histories are similar to those obtained when evaluating different cooling temperatures. Additionally, the effects of solar insolation are seen to lead only to small changes in the maximum flange temperature. This can also be

attributed to the fact that solar insolation effects are present only during the later portion of the thermal test when the flange temperature has already reached its maximum. As in the cooling temperature scenarios, the C9 thermal test provided a conservatively high estimate of the maximum flange temperature. A final simulation was also conducted using the worst possible conditions. Here a $120 \text{ W}/m^2$ internal heat source was used with cooling in a 120°F environment under a solar flux of $300 \text{ W}/m^2$. Again the C9 thermal test provided a conservative measure of the maximum flange temperature.

The previous analysis indicates that the maximum flange temperature determined in the C9 thermal test on pre-heated empty shipping containers is greater than the temperature expected for filled containers with an internal heat source. Additionally, the analysis showed that the C9 thermal tests, as performed, overpredicts the maximum flange temperature reached in a number of different scenarios that meet or exceed Federal regulations. The flange temperature served as a measure of the temperature reached by the O-ring which is the most temperature sensitive part of the shipping container. The extent to which the C9 thermal test overpredicted the maximum flange temperature decreased with time. The speed at which this process occurred depended on the thermal boundary conditions present. It was also determined that the flange temperature is most sensitive to the heat generated by the foam fire, a phenomena that is taken into account in a crude but effective manner in this analysis.

Intentionally Left Blank

References

- [1] General Plastics Mfg. Co. - Product Specification Sheet. <http://www-generalplastics.com/warranty.html>, 2002.
- [2] *Code of Federal Regulations*. 10 CFR 71: Packaging and transportation of radioactive material. 1995.
- [3] Frank P. Incropera and David P. DeWitt. *Fundamentals of Heat and Mass Transfer*. John Wiley and Sons, 1990.
- [4] Y. Ohashi and A. R. Ortega. H1616-1 container post-fire solar insolation thermal analysis. Internal Memo from Y. Ohashi and A. R. Ortega to B. E. Oden, 2002.
- [5] John C. Tannehill, Dale A. Anderson, and Richard H. Pletcher. *Computational Fluid Mechanics and Heat Transfer*. Taylor and Francis, 1997.
- [6] G. G. Tipton and A. R. York. Safety analysis report for the type B (U) AL-SX (H1616) reservoir packages. Technical Report SAND 91-2205, Revised, Sandia National Laboratories, 1996.

DISTRIBUTION:

1	MS 9001	M.E. John, 8000	
		Attn: P.N. Smith, 8500	MS 9002
		K.E. Washington, 8900	MS 9003
1	MS 9004	J. Vitko, 8100	
		Attn: A. McDonald, 8118	MS 9105
		W.R. Bolton, 8120	MS 9104
		L.M. Napolitano, 8130	MS 9951
		D.L. Lindner, 8101	MS 9951
		L.D. Brandt, 8112	MS 9201
		P.K. Falcone, 8114	MS 9201
1	MS 9007	D.R. Henson, 8200	
		Attn: Monson, 8243	MS 9108
1	MS 9108	B. Oden, 8243	
1	MS 9108	G.C. Story, 8243	
1	MS 9054	W.J. McLean, 8300	
		Attn: L.A. Rahn, 8351	MS 9051
		D.R. Hardesty, 8360	MS 9052
		R.J. Gallagher, 8361	MS 9052
		J.O. Keller, 8362	MS 9053
1	MS 9045	R.H. Stulen, 8700	
		Attn: K.L. Wilson, 8703	MS 9402
		W. Bauer, 8704	MS 9161
		R.Q. Hwang, 8721	MS 9161
		W.R. Even, 8722	MS 9402
		J.C.F. Wang, 8723	MS 9403
		C.H. Cadden, 8724	MS 9402
		J.R. Garcia, 8725	MS 9404
		E-P Chen, 8726	MS 9161
		C.C. Henderson, 8729	MS 9401
		J.E.M. Goldsmith, 8730	MS 9409
		W.C. Replogle, 8731	MS 9409
		G. Kubiak, 8732	MS 9409

1	MS 9401	J.M. Hruby, 8702	
1	MS 9042	D.R. Chenoweth, 8728	
1	MS 9042	A. Dryden, 8728	
1	MS 9042	G.H. Evans, 8728	
1	MS 9042	S. Griffiths, 8728	
5	MS 9950	J.T. Hollenshead, 8728	
1	MS 9042	W.G. Houf, 8728	
1	MS 9042	M.P. Kanouff, 8728	
1	MS 9042	R.S. Larson, 8728	
1	MS 9042	C.D. Moen, 8728	
1	MS 9042	R.H. Nilson, 8728	
1	MS 9401	B.M. Rush, 8728	
1	MS 9401	W.B. Tauber, 8728	
1	MS 9950	S.W. Tchikanda, 8728	
1	MS 9042	A. Ting, 8728	
1	MS 9950	G.J. Wagner, 8728	
1	MS 9042	W.S. Winters, 8728	
1	MS 9042	A.R. Ortega, 8727	
1	MS 9042	Y. Ohashi, 8727	
1	MS 0841	T.C. Bickel, 9100	
		Attn: M.J. McGlaun, 9140	MS 0835
		A.C. Ratzel, 9110	MS 0824
		W.H. Rutledge, 9115	MS 1174
		E.S. Hertel, 9116	MS 0836
		W.L. Hermina, 9113	MS 0826
		J.E. Johannes, 9114	MS 0834
		R.O. Griffith, 9117	MS 0836
		S.N. Kempka, 9141	MS 0835
3	MS 9018	Central Technical Files, 8945-1	
1	MS 0899	Technical Library, 9616	
1	MS 9021	Classification Office, 8511	
		Attn: Technical Library, 9616	MS 0899
		DOE/OSTI via URL	

Intentionally Left Blank